Annual Report
Hydrospheric Atmospheric Research Center (HyARC)
Nagoya University

2013

Contents

Foreword

During summer of year 2013, it was very hot and also it rained heavily breaking records in many places in Japan. Many people suffered damages caused by typhoon and other water related disasters, such as floods and landslides, possibly related to global warming. Many of members of Hydrospheric Atmospheric Research Center (HyARC) were very busy for research projects and contributions to society during this year. Specifically, members of the laboratory of meteorology doing modeling and observations of extreme weather faced busy schedules such as TV interviews.

As a Joint Usage/Research Center, 25 collaborations for 5 planned researches and 4 workshops were conducted. Cloud and rain particles just before becoming typhoon was observed by Multi-parameter radar system and cloud particle sonde in Republic of Palau as a collaborative research with Japan Agency for Marine-Earth Science and Technology and other organizations. Ka-band radar for observation of inside of cloud, which was requested several years, was accepted at the end of 2012 and introduced this year.

As international activities, MOU with Taiwan Ocean Research Institute for research to use ocean HF radar was extended, and it is decided to sign a MOU with Korean Ocean Satellite Center of Korea Institute of Ocean Science and Technology for verification and use of ocean color satellite data. Associate Professor Tomo'omi Kumagai was honored to be invited by His Royal Highness The Prince of Whales to the meeting at the Royal Society and at St. James's Palace for "St. James' Palace memorandum on Tropical Forest Science" with other famous scientists.

HyARC stuffs also contributed to the education. 10 master and 3 Ph.D students of Graduate School of Environmental Studies were finished their degree courses with supervised by stuffs of HyARC. Mr. Tomonori Tsujino awarded best student presentation award of Hydrospheric and Atmospheric Science section of Japan Geosciences Union Meeting 2013. Global COE program lead by Prof. Tetsuzo Yasunari was completed, and two stuffs are now participating "Leadership Development Program for Space Exploration and Research" conducted mainly by Graduate Schools of Science and Engineering and Solar-Terrestrial Environmental Laboratory (STEL). Beautiful pictures were taken at the stratosphere with a smart phone on a sonde during an event of "Anomalo goes to Space" conducted by Laboratory of Meteorology, Gamagori Network Research Center Natural History Museum –Sea of Life- and Nagoya Institute of Technology.

From 2012 to 2013, HyARC is entering a phase of major change. Most of the stuff moved to 6 and 7th floors of a new building with STEL and EcoTopia Science Institute (EcoTopia) from the scattering temporal spaces stayed during latter 2012. This building was name as Research Institutes Building. The old building built on 1969 during Water Quality Science Research, Faculty of Science was mostly abandon to the stuff of Hydrospheric-Atmospheric group of Graduate School of Environmental Studies. The new building is very comfortable and can be saved the expenses of utilities. Construction of the second Research Institutes Building has been started for EcoTopia, STEL, HyARC as well as Center for Chronological Research (CCR). Administration office of HyARC was also changed from the Graduate School of Environmental Studies to the same office of STEL and EcoTopia. It is further expected that the collaboration of the research will be also enhanced with STEL after the sharing of the building and administration office together.

Prof. Kenji Nakamura, former director and worked hard for change from the Institute for Hydrospheric-Atmospheric Sciences to HyARC, was retired. From 2013, Prof. Joji Ishizaka became the director, and Assistant Prof. Taro Shinoda became Associate Professor. Furthermore, Endowed Research Division of Stakeholder Management Research Laboratory was established with the limit of

two years. For this laboratory, Prof. Kimiaki Yasuda, Assistant Prof. Memi Motosu and special-appointment Prof. Eiichi Tanoue was arrived. It was decided that Dr. Tetsuya Hiyama, who lead a project in Research Institute for Humanity and Nature, will come back from 2014. Therefore, HyARC is now within large changes for personnel affairs too.

During the large changes, the mid-term evaluation by Ministry of Education, Culture, Sports, Science and Technology (MEXT) in early 2013 was conducted, followed by the evaluation of department by the university and the external evaluation. Unfortunately, the evaluation of the MEXT was not as good as we believed. We are now starting the reformation in many ways. One of the possibilities of the drastic change is the formation of new institution with STEL and CCR are started discussion.

We are now searching a new direction in order to enhance support of the community, such as Japan Meteorological Society, Japan Oceanographic Society, and Japan Society of Hydrology and Water Resources who endorsed the HyARC, and preparing to new certification of the Joint Usage/Research Center. We hope the scientific communities provide us the warm advice and guidance.

Ishizaka Joji
Director
Hydrospheric Atmospheric Research Center

Staff and Organization

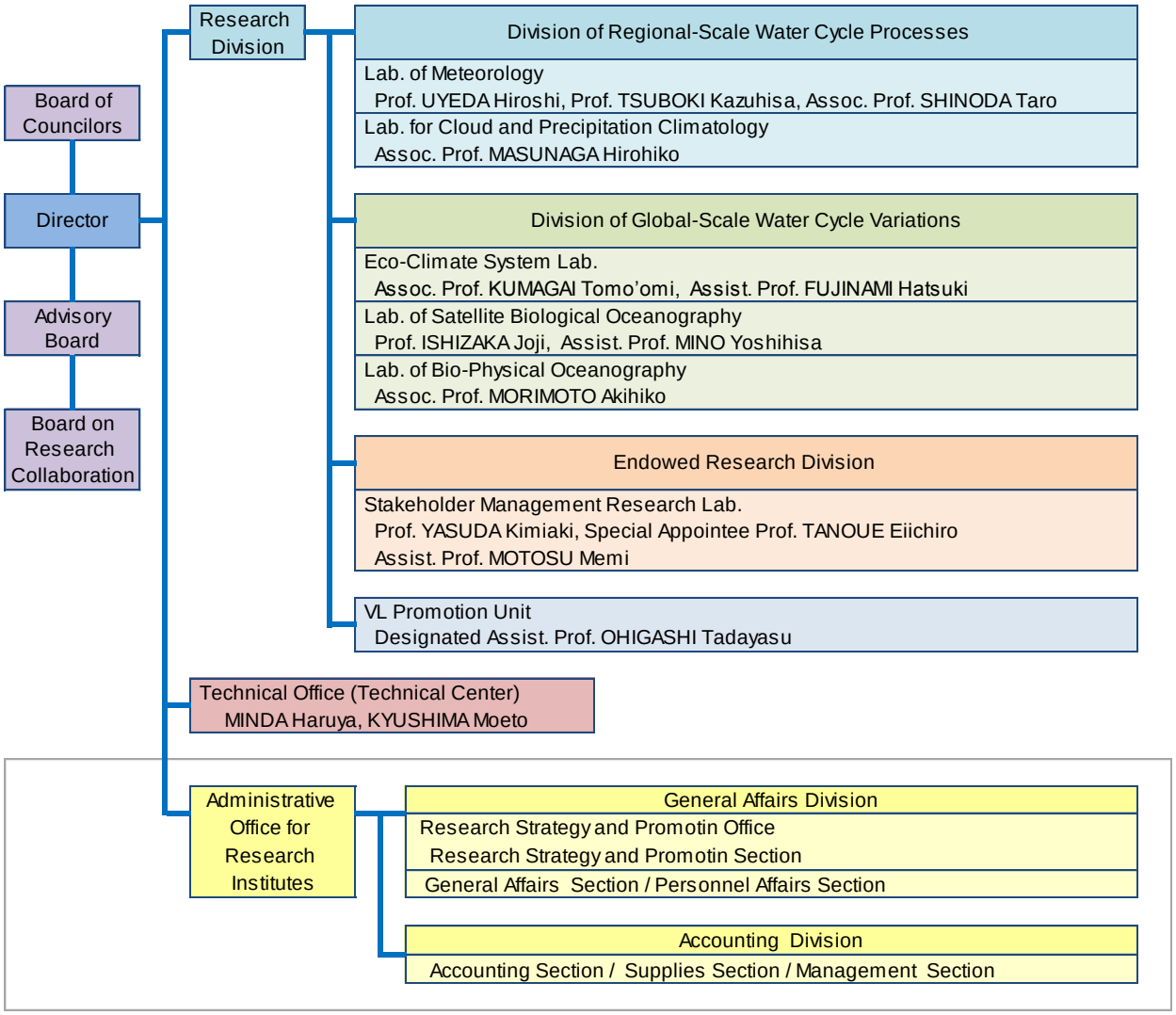

Administration

Board of Councilors

●Members from Nagoya Universituy

TANAKA Kentaro: Prof., Graduate School of Science
TSUJIMOTO Tetsuro: Prof., Graduate School of Engineering
TAKENAKA Chisato: Prof., Graduate School of Bioagricultural Sciences
KANZAWA Hiroshi: Prof., Graduate School of Environmental Studies
MATSUMI Yutaka: Prof., Solar-Terrestrial Environment Laboratory
ISHIZAKA Joji: Director, Prof., Hydrospheric Atmospheric Research Center
UYEDA Hiroshi: Prof., Hydrospheric Atmospheric Research Center
TSUBOKI Kazuhisa: Prof., Hydrospheric Atmospheric Research Center

Advisory Board

●Members from outside of Nagoya University

FUJIYOSHI Yasushi: Prof., Institute of Low Temperature Science, Hokkaido University
HANAWA Kimio: Prof., Graduate School of Science, Tohoku University
TERASHIMA Ichiro: Prof., Graduate School of Science, The University of Tokyo
NAKAMURA Kenji: Prof., Department of Economics on Sustainability, Dokkyo University
SUMI Akimasa: President, National Institute for Environmental Studies
YAMANAKA Manabu: Principal Scientist, Research Institute for Global Change, Japan Agency for Marine-Earth Science and Technology
TANIGUCHI Makoto: Prof., Research Institute for Humanityand Nature
OKI Riko: Senior Researcher, Earth Observation Research Center, Japan Aerospace Exploration Agency

●Members from HyARC, Nagoya University

UYEDA Hiroshi: Prof., Hydrospheric Atmospheric Research Center, Nagoya University
TSUBOKI Kazuhisa: Prof., Hydrospheric Atmospheric Research Center, Nagoya University
ISHIZAKA Joji: Prof., Hydrospheric Atmospheric Research Center, Nagoya University
MASUNAGA Hirohiko: Assoc. Prof., Hydrospheric Atmospheric Research Center, Nagoya University
KUMAGAI Tomo'omi: Assoc. Prof., Hydrospheric Atmospheric Research Center, Nagoya University
MORIMOTO Akihiko: Assoc. Prof., Hydrospheric Atmospheric Research Center, Nagoya University

Board on Research Collaboration

●Members from outside of Nagoya University

FUJIYOSHI Yasushi: Prof., Institute of Low Temperature Science, Hokkaido University
YAMANAKA Manabu: Principal Scientist, Research Institute for Global Change, Japan Agency for Marine-Earth Science and Technology
TANIGUCHI Makoto: Prof., Research Institute for Humanityand Nature
OKI Riko: Senior Researcher, Earth Observation Research Center, Japan Aerospace Exploration Agency

●Members from Nagoya University

UYEDA Hiroshi: Prof., Hydrospheric Atmospheric Research Center, Nagoya University
TSUBOKI Kazuhisa: Prof., Hydrospheric Atmospheric Research Center, Nagoya University
MASUNAGA Hirohiko: Assoc. Prof., Hydrospheric Atmospheric Research Center, Nagoya University

Stakeholder Management on Offshore Wind Endowed Research Division Steering Committee

●Members from outside of Nagoya University

FUJIYOSHI Yasushi: Prof., Institute of Low Temperature Science, Hokkaido University

●Members from Nagoya University

KANZAWA Hiroshi: Prof., Graduate School of Environmental Studies, Nagoya University
YASUDA Kimiaki：Prof., Endowed Research Division Professor, Hydrospheric Atmospheric Research Center, Nagoya University
MATSUMI Yutaka: Prof., Solar-Terrestrial Environment Laboratory, Nagoya University
ISHIZAKA Joji: Director, Prof., Hydrospheric Atmospheric Research Center, Nagoya University
UYEDA Hiroshi: Prof., Hydrospheric Atmospheric Research Center, Nagoya University
TSUBOKI Kazuhisa: Prof., Hydrospheric Atmospheric Research Center, Nagoya University
MORIMOTO Akihiko: Assoc., Prof. Hydrospheric Atmospheric Research Center, Nagoya University

Research Program

Satellite Data Simulators and their application to numerical model evaluation

A satellite simulator is a computer program that reproduces satellite-observed radiances or radar echoes by applying radiative transfer computations to temperature and humidity profiles and cloud and precipitation fields generated by numerical models such as cloud-resolving modes and general circulation models. We develop and distribute the Satellite Data Simulator Unit (SDSU) at HyARC and, as an effort for its applications, conduct an evaluation study of the cloud microphysical schemes for CReSS. This research program is aimed at strengthening the link between the satellite simulator developers and existing and new users across the country. In this year, which is the first year of this program, we began new collaborations with the Joint-Simulator developer team lead by Prof. Masaki Satoh at AORI of University of Tokyo and the JMA Meteorological Satellite Center team in charge of the data product for the next generation Geostationary Meteorological Satellites.

A joint workshop on GSMaP and satellite simulators was held together with the GSMaP developer group on February 18th and 19th, 2006. Scientists specializing in broad areas of satellite meteorology participated in this workshop, leading to further reinforcement of our confidence that HyARC are and will be playing a pivotal role in the relevant research community in Japan.

Multi-scaled vegetation-climate interaction -from a leaf to continents

In this research project, to clarify resilience and variation characteristics of land-climate interactions in terms of hydrologic climatic processes, we showed the significance of vegetation (terrestrial ecosystems) in the climate system. In this year, several groups joined our projects and conducted their own subprojects. The results are as follows:

Some historical climatic data analyses and numerical modelling researches revealed that impacts of land-use changes on vegetation-climate interactions should be involved in causes for long-term and large-scale changes in Asian monsoon activity.

Some promising methods for high-accurate evaluation of temporal and spatial variation in vegetation status were examined using everyday-observations of ecological phenology and cloud cover at a super-site in Asian tropical rainforests. Items of the observations were GRVI (Green-Red ratio Index) estimated from multi-satellites remote sensing data and phenology images captured by digital cameras, found to be very effective for accurately detecting forest destruction and degradation caused by both human activity and natural disaster.

To directly detect the impact of climate change on vegetation ecosystems, a group has observed temporal variations in *Fraxinus platypoda* flowering at two super-sites for more than 20 years. They revealed that changes in trends of the flowering patterns were mainly attributed to local or/and global climate change.

Research on Coast Circulation, Biological Production and Material Transport with Remote Sensing

Coastal area is between land and open ocean, and high biological production, active circulation and material transport are maintained by freshwater input with materials from land, including human origin, and by physical variations affected by topography. Because it is difficult to access to oceanic area, unlike on land, observation by remote sensing is very important. However, satellite sensors covering and resolving typical time and spatial scales in coastal area are limited, and remote sensing of coastal area is not fully operational because many technical problems still remain.

Scientists in Hydrospheric-Atmospheric Research Center have conducted research on development of remote sensing data and analysis of the data in coastal area, such as development of verification system of primary production, estimation and behavior of chlorophyll and suspended maters in East China Sea, red tide in Japanese coastal area, circulation in the East China Sea using sea surface topography and HF radar data. Japan Aerospace Exploration Agency (JAXA) is proposing new ocean color and sea surface topography sensors, and it is expecting that activities of remote sensing user community for coastal environment will be expanded.

Research program, "Research on Coast Circulation, Biological Production and Material Transport with Remote Sensing", has been started from 2011, and five collaborative research programs were accepted and conducted for 2013 as followings.

- 10th Korea-Japan Workshop on Ocean Color Remote Sensing was held as Asian Workshop on Ocean Color 2013 on Dec 3-5, 2013, in Taiwan, and it was decided to make an agreement of research between HyARC and Korea Ocean Satellite Center.
- Chlorophyll-a measurements of Ise Bay and Biwa Lake by ocean color remote sensing and current measurements in Tsushima Strait was established.
- Accurate tidal model was developed with data assimilation of satellite and tidal data on numerical model.

Development of remote sensing technology for atmosphere and ocean phenomena

We have set up ocean Radar sites in Tsushima of Nagasaki Prefecture and Aishima of Yamaguchi Prefecture in FY 2013. The ocean Radar sites consist of 15 or 14 array of 2 elements Yagi as receiving antenna, 3 elements Yagi as transmitting antenna, and a container which is put up radio and PCs. Electric power and communication have been supplied, and it is final adjustment stage for continuous operation. We will observe sea surface current field vicinity of Tsushima Straits for 3 years. In addition, we will develop a new type of ocean Radar with NICT, Ryukyu University, National Fisheries University, and Kyushu University.

We promote the preparation of ocean Radar observation in Wakasa Bay in order to understand mechanism of sudden strong current in the Bay. The sudden strong current called “Kyucho” occurs especially in summer in Wakasa Bay, which causes damage to fisheries industry in the Bay. It is suggested that Kyucho is caused by a clockwise circulation in the Wakasa Bay associated with the Tsushima Warm Current approaching to Wakasa Bay. However, generation mechanism of the Kyucho is not evident at the moment. We made a research plan to capture the circulation in the Bay using ocean Radar which measures sea surface current within 70km from the Radar site.

Advanced utilization of the polarimetric radars and the cloud-resolving model for cloud and precipitation research

The research program is aiming at a research frontier of cloud and precipitation physics by advanced utilization of various polarimetric radar parameters and the cloud-resolving model. In this year, 12 principal investigators (PIs) performed the following researches in the research program. Some researches made further development of the CReSS model and related program codes. In these research, an ocean model and wave model were incorporated into CReSS. In particular, the CReSS model was applied to the Mars atmosphere. CReSS was used for a regional weather prediction in Aizu University. Daily weather prediction using CReSS has been performed at HyARC and that in a new region started. CReSS was also used for a research of transportation of pollution.

The polarimetric radar of Nagoya University was installed in Palau and used for a research of tropical precipitation systems. Some of PIs of the HyARC research program joined the radar observation program in Palau led by Prof. Uyeda and a collaboration was performed in the tropical region.

A data assimilation research using CReSS and radar was performed in the program. The assimilation of radar data to the CReSS model increase the accuracy of prediction of thunderstorms. The data assimilation is a promising technique to combine observation and modeling. We expect that the technique will be apply to various research of cloud and precipitation.

Formation of a virtual laboratory for diagnosing the earth's climate system (VL)

To conduct collaborate research and education in addressing a diagnosis of the earth's climate system being under great stress such as global warming, "The virtual laboratory (VL) for diagnosing the earth's climate system" was formed in 2007 by the four university research centers studying climate and environment. HyARC sets up "Atmospheric Research Promotion Team (VL Promotion Team)" and mainly studies water budget associated with cloud and precipitation and develops an observation and analysis system. To be concrete, we analyze two X-band polarimetric Doppler radar data for diagnosing a category of hydrometeor particles, develop a cloud-resolving model named Cloud Resolving Storm Simulator (CReSS) and validate its results using a satellite simulator named Satellite Data Simulator Unit (SDSU), and establish data assimilation method on a mesoscale precipitation system.

In 2013, we conduct a field observation using a polarimetric Doppler radar and hydrometeor videosondes (HYVISs) in Republic of Palau in June to clarify the formation process of initial vortices of tropical cyclones (TCs) and contribution of cloud microphysical processes on the formation of TCs. The other radar have installed at Kobe International University to observe thunderstorms over the Osaka Plain.

Comparison in brightness temperature (TBBs) of infrared and reflectivity obtained from satellite observations with those calculated by SDSU applied to the daily simulation results using CReSS is carried out. We focus on the evaluation of number concentration of cloud ice in the upper troposphere. Simulated area less than 220 K in TBBs of infrared band corresponding to upper anvil clouds is greater than the observed one (not shown). Figure shows vertical cross section of observed reflectivity for 94 GHz obtained by CloudSat-CPR and that of simulated one. Simulated weak reflectivity region in the upper troposphere that corresponds upper anvil clouds extends narrower than the observed one. These results are attributed to greater number concentration of cloud ice in the simulation, thus the simulated particle size of cloud ice is smaller than the observed one. This results suggests that the ice nucleation process in the CReSS model should be improved.

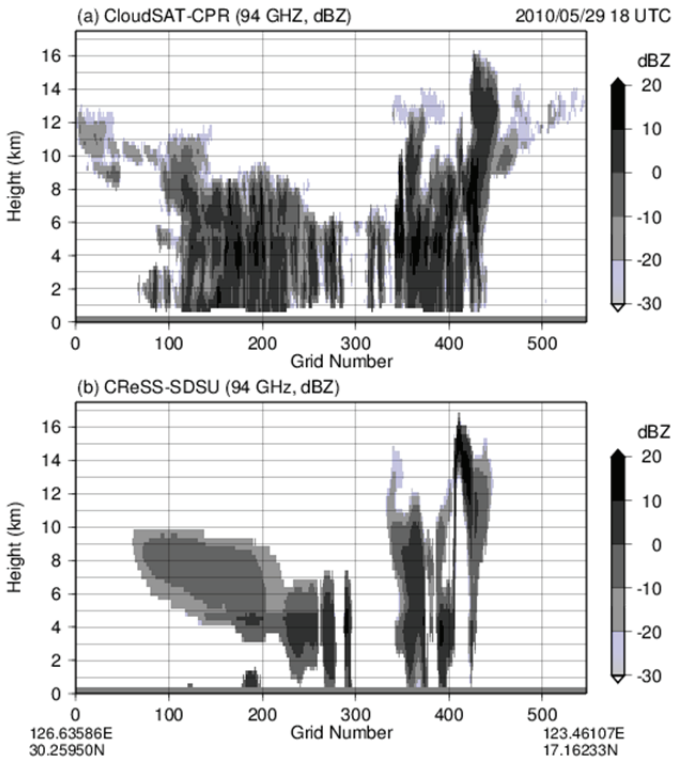

Fig. 1: Vertical cross section of (a) observed reflectivity for 94 GHz obtained by CloudSat-CPR and (b) simulated one (CReSS-SDSU) over the Taiwan-Okinawa region at 18 UTC on May 29, 2010.

Core Research for Evolutional Science and Technology (CREST)

Development of a method to comprehend and predict wind conditions required for offshore wind-power generation

Research Project "Development of a method to comprehend and predict wind conditions required for offshore wind-power generation" (Research director: Prof. H. Uyeda, Nagoya University) started from October 2012 for two and a half years. The research is one of topics in the research area of "Creation of fundamental theory and technology to establish a cooperative distributed energy management system and integration of technologies across broad disciplines toward social application" in the Japan Science and Technology Agency/Core Research for Evolutional Science and Technology (JST/CREST). Strategic object of the research area is the creation of theory, mathematical model, and fundamental technology to establish a cooperative distributed energy management system, which enables the optimization of demand and supply for various energies including renewable energy. Offshore wind-power generation is one of the plausible ways to supply renewable energy.

Understanding of offshore wind conditions are required in order to promote the business of offshore wind power generation capable. However, from the difficulty of observation, available data is limited. Under these circumstances, year-round observations of offshore wind conditions off Wajima, west coast of Japan, have been started from November 24, 2010. The data of three wind observation towers (50 m height) in Hegura-jima and in two other sites along the coast are provided to the research group at Nagoya University. On the other hand, a very high-resolution simulation is necessary for estimation and prediction of offshore wind power. To perform such a high-resolution simulation with explicitly-calculating convective clouds, we use a cloud-resolving model named the Cloud Resolving Storm Simulator (CReSS) developed by Tsuboki and Sakakibara (2002). A detailed cloud microphysics and an atmospheric turbulence are considered in the model. It has been used for real weather prediction with high resolution. In the present study, estimation and prediction of offshore wind power were performed using CReSS. The performance of the CReSS for simulating offshore wind is confirmed in comparison with the tower data in Hegura-jima as shown in Fig. 1. The output data of calculations will be used for an estimation of offshore electric power to be generated by wind turbines in collaboration with Prof. Morinishi group, Nagoya Institute of Technology. The developer of CReSS, Prof. Tsuboki, Nagoya University, is seeking for new studies on estimation, prediction and utilization of offshore wind for the next five years.

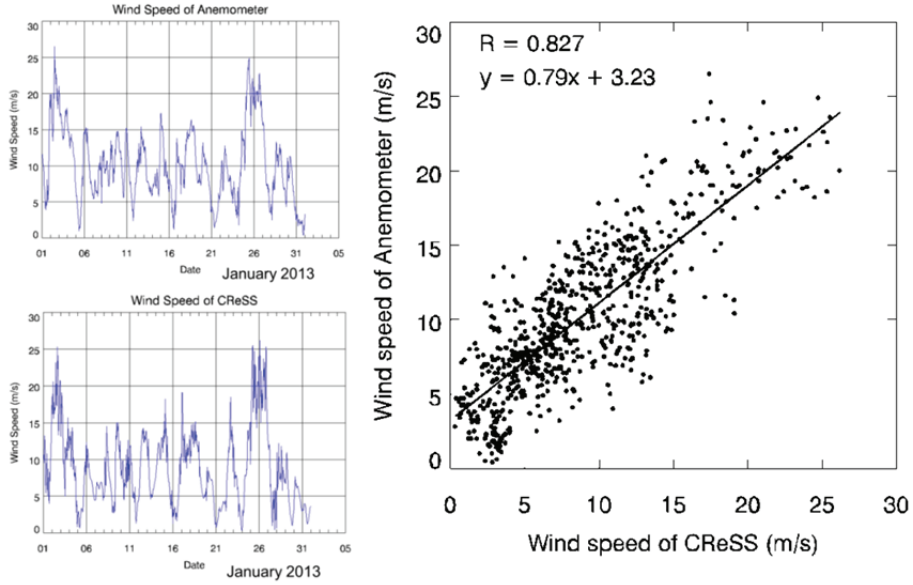

Fig. 1 : Comparison of wind speed of anemometer at the height of 50 m on a wind tower in Hegura-jima and CReSS simulation of 2 km x 2 km horizontal resolution for the anemometer point: time variation of wind speed for January 2013 of anemometer (left top panel) and that of CReSS simulation (left bottom panel), and scatter plot of them (right panel).

Program for Risk Information on Climate Change (SOUSEI Program)

Development of coupled ocean-atmosphere non-hydrostatic model for typhoon research

A super-typhoon, the most intense tropical cyclone category in the western North Pacific, occurs infrequently, but its landfall causes catastrophic disaster. The purpose of our research group is more accurate estimation of the maximum possible intensity of typhoon in the future climate using a numerical model. In 2013, we developed a coupled atmosphere-wave-ocean non-hydrostatic model, CReSS-NHOSE with a wave model (Figure 1). The exchange of momentum between the atmosphere and the ocean is performed by the wave model. Consequently, the maximum surface wind region is not necessary to coincide with the region of maximum wave height and the wind direction is not necessary to be the same as the direction of wave propagation. We also incorporated the ocean mixing layer model which was developed by the Hibiya's group in the Kakushin Program. The first step of the coupled model development was completed. Using the coupled mode, daily simulation experiment is performed for the domain including the main part of the Kuroshio current in the western North Pacific. We also performed nine typhoons in 2012 and 2013 to examine the effect of coupling the ocean model for typhoon simulation. The maximum difference between the coupled model and the atmospheric model was 10 hPa. The simulation results using the coupled model were compared with an ocean observation to verify the model performance. The results show that the modification of the ocean mixing layer due to the passage of a typhoon and the Kuroshio current to the northeast of Taiwan were successfully simulated. The atmospheric part of typhoon simulation was compared with drop-sonde observations. The thermodynamic structures such as temperature and moisture around the typhoon center showed a good agreement with the observations. Besides, simulation experiments of the super-typhoon Haiyan (2013) and the typhoon Bolaven (2012). Using cloud-resolving models, CReSS and MRI-NHM, we performed downscale simulation experiments of vary intense typhoons simulated by the MRI-AGCM20km in the future climate. The horizontal grid spacing was 2 km in the downscale experiments. The life-time minimum sea level pressure of the simulated typhoons is often lower than that of the AGCM and the theoretical maximum possible intensity. Both models showed similar results. This increases the reliability of the downscale simulations.

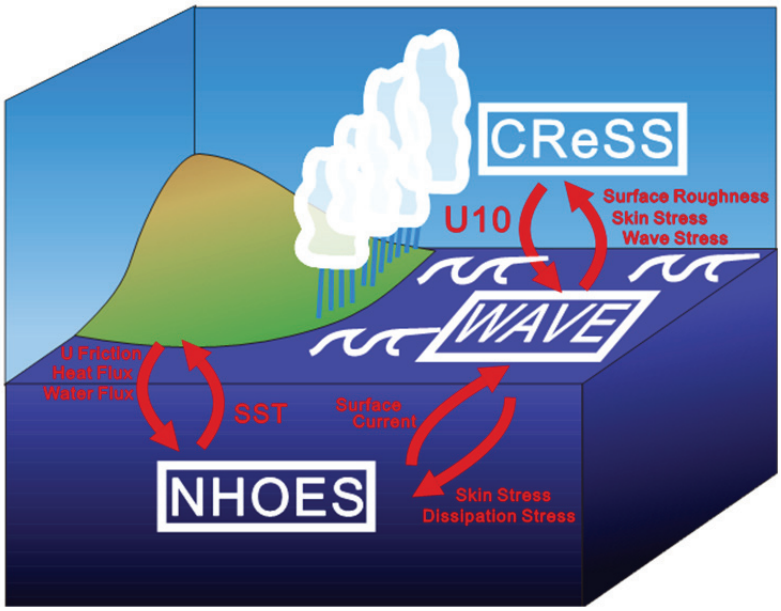

Fig. 1 : Schematic representation of the Coupled Atmosphere-Wave-Ocean Non-hydrostatic Model (CReSS-NHOSE).

Program for Risk Information on Climate Change (SOUSEI)

Eco-climate system in Northeastern Eurasia and Southeast Asian tropics: impacts of global climate change

We are conducting predictions and assessments on how climate change alters forest vegetation and then whether the altered forest vegetation affects the climate. The main research sites are in Asian rainforests and the eastern boreal Siberia. We are studying the changes in the major forests in the world, such as the tundra forest.

One of this year's results is as follows: Rubber (*Hevea brasiliensis* Müll. Arg.) plantations are a viable resource for the economics of Southeast Asian countries. They are rapidly expanding into both climatically optimal and sub-optimal environments throughout mainland Southeast Asia, potentially changing the partitioning of water, energy, and carbon at multiple scales, compared with traditional land covers that are being replaced. To provide a useful tool for a resource management strategy for rubber plantation agriculture, e.g., balancing rubber plantation productivity with the need to reduce the environmental impacts associated with agricultural development, we developed the Spatially Explicit Individual-Based (SEIB) Dynamic Global Vegetation Model (DGVM) applicable to simulating both primary productivity and latex productivity in rubber plantations (R-SEIB: Fig. 1). R-SEIB can take the climatic impacts on productivity processes into consideration, and thus, allows us to project future rubber plantation productivity under climate change conditions. In this study, model results were compared with measurements collected at a field site in central Cambodia, and after validating the R-SEIB's performance, we conducted numerical experiments addressing rubber plantation management issues, revealing insights, such as the effects of enhanced photosynthetic ability on latex productivity and the relationships between latex tapping interval and tree growth rate and the timing of plateau of the above-ground biomass and latex production.

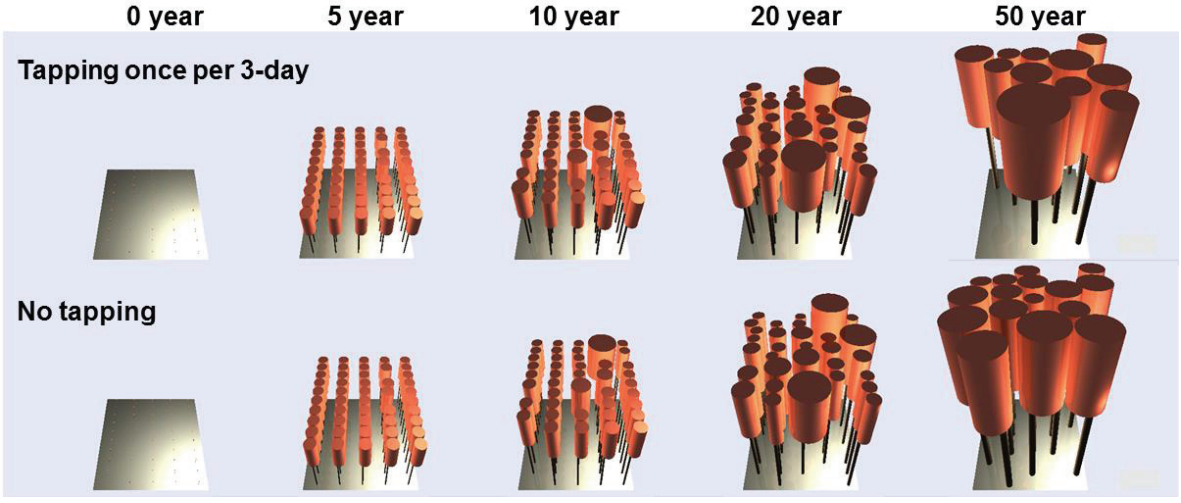

Fig. 1 : Simulation results of 30 m×30 m rubber plantation dynamics for 50-years at a Cambodian site.

Laboratory of Meteorology

Vortex structure and development process of parent storm of a tornado occurred in Inabe City, Japan

A tornado struck Inabe City, central Japan, at about 15 JST on September 18, 2012. This event is referred to as "Inabe tornado" in this study. The parent storm of the Inabe tornado developed in the humid environment in which tornadoes occur occasionally in Japan. The purpose of this study is to reveal characteristics of a tornado and its parent storm in the humid environment, by a case study of the Inabe tornado. In particular, this study focuses on the vortex structure and development process of the parent storm using three X-band polarimetric radars that covers Inabe city.

Vertical vortices are detected by a method proposed by Donaldson (1970) and Suzuki et al. (2000) to apply the plan position indicator (PPI) data of each elevation angle of all radars. Vertical velocity is estimated by dual-Doppler analysis on a Doppler velocity field obtained by all radars.

Since a mesocyclone whose diameter of approximately 4 km is identified within the parent storm, the Inabe tornado is recognized to be associated with a supercell type storm. A hook echo, weak-echo region under an echo overhang, which are typically observed in the supercell storm over the Great Plains are detected in the parent storm. The updraft velocity in a core of the parent storm is approximately 14 m s^{-1} at a height of 2 km (Fig. 1), and is weaker than typical supercells over the Great Plains. Cold outflow produced by a downdraft in the core with wind speed of 10 m s^{-1} at a height of 1 km is balanced with the warm and moist southeasterly inflow. A smaller scale vortex referred to as “misocyclone” is detected within the mesocyclone. A misocyclone is observed adjacent to the mesocyclone a few minutes before the occurrence of the Inabe tornado. It is noteworthy that a pair of positive and negative vortices with the diameter about 1-3 km is detected in a rear-flank of the parent storm before the appearance of the misocyclone.

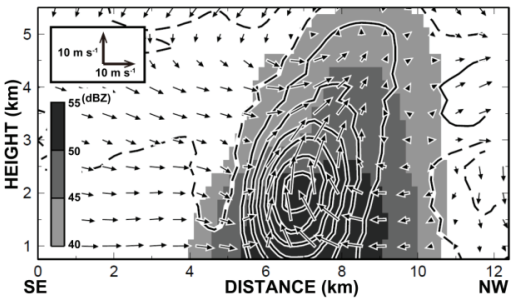

Fig. 1 : Vertical cross section of reflectivity (shading), vertical velocity (contour), and storm-relative wind velocity (vectors) on the plane along an inflow through the core of the updraft at 1505 JST. The thick and dashed contours indicate updraft and the downdraft every 2 m s^{-1} starting from 1 m s^{-1}, respectively.

Figure 2 shows schematic images of the structure of the parent storm of the Inabe tornado. A vortex pair is formed by the tilting of the horizontally elongated vortex tube that has horizontal vorticity by an updraft associated with a rear-flank downdraft and cold outflow. The cyclonic vortex of the vortex pair moves into the mesocyclone just before the deep development of the misocyclone. As the location of the misocyclone in the parent storm corresponds to the damage track of the Inabe tornado, we propose that the formation of the Inabe tornado is attributed to the regional intensification of an updraft by the misocyclone.

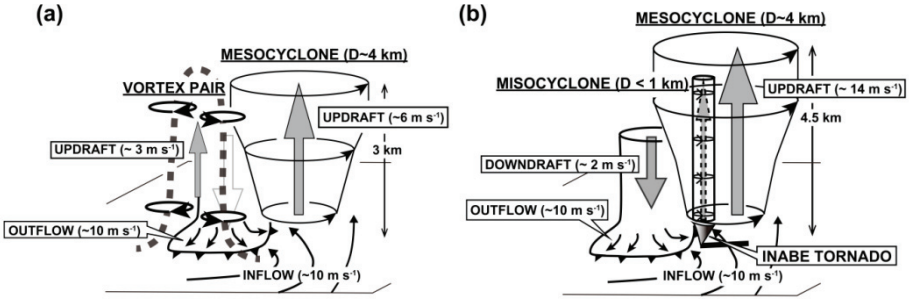

Fig. 2 : Schematic images of the structure of the parent storm of the Inabe tornado at the stage of (a) the formation of the vortex pair and (b) the development of the misocyclone. The thick arrows indicate updraft and downdraft. The thin arrows indicate the storm-relative wind. The circular arrows indicate the vortex detected by radars. The thick line in (b) indicates the damage track of the Inabe tornado.

Distribution of solid particles in precipitation systems during the Baiu season in Okinawa

To clarify precipitation mechanisms in mesoscale precipitation systems during the Baiu season, distributions of solid particles, such as ice crystals, snowflakes, and graupels, above melting level should be investigated. In this study, we reveal vertical distribution of hydrometeors using data obtained by an X-band polarimetric radar installed at Aguni Island, Okinawa Prefecture. We use total 1392 data of range height indicator (RHI) obtained in 36 days from May 23, 2011 and in 41 days from May 7, 2012.

First we exclude the case that echo-top height is lower than the melting level (approximately at a height of 5 km), and 548 cases still remain. Precipitation systems are divided into 3 types. "A stratiform precipitation system" is defined by the criteria: Echo-top height of 30 dBZ does not exceed above the melting level and a significant bright band is detected. "An isolated convection" is defined by that: Echo-top height of 30 dBZ exceeds above the melting level and no significant bright band is detected. "Convective cells embedded in a stratiform precipitation system" is defined by that: Echo-top height of 30 dBZ exceeds above the melting level and a significant bright band is detected. Figure 3 shows a sample of the three types. According to the definition, 465, 23, and 60 cases are classified into a stratiform precipitation system, an isolated convection, and convective cells embedded in a stratiform precipitation system, respectively. Thus precipitation during the Baiu season in Okinawa is expected to be mainly brought about by a staratiform precipitation system.

A hydrometeor classification analysis is applied to all of the RHI data and vertical distribution of frequency of each solid particle; ice crystal, dry snow, and dry graupel, is analyzed for each type of the precipitation system (Fig. 4). Frequency of ice crystal and dry snow is dominant through all types of the precipitation system above the melting level. Dry graupel is detected very few in a stratiform precipitation system. On the other hand, dry graupel is detected below 11 km and its frequency exceeds 35% at a height of 5.5 km (around the melting level) in an isolated convection. Since frequency of an isolated convection and convective cells embedded in a stratiform precipitation system is quite few in comparison with that of a stratiform precipitation system, the contribution of graupel to produce a heavy rainfall event is expected to be small during the Baiu season in Okinawa. As a result, the coalescence process of raindrops should be mainly attributed to produce a heavy rainfall in the precipitation mechanism.

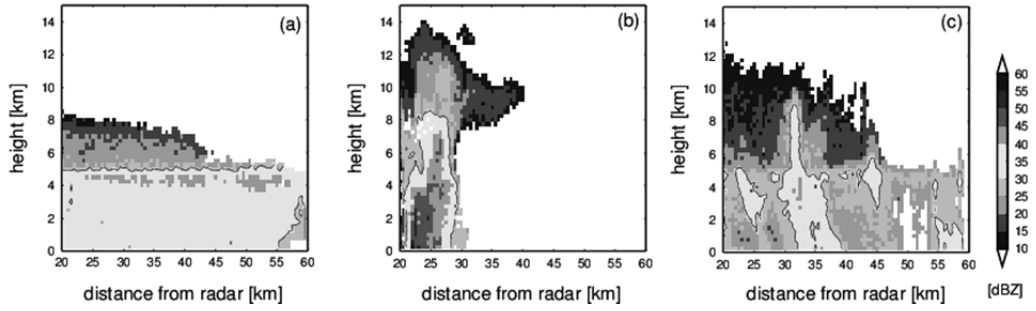

Fig. 3 : A sample of RHI images of reflectivity for 3 types of the precipitation system: (a) a stratiform precipitation system, (b) an isolated convection, and (c) convective cells embedded in a stratiform precipitation system.

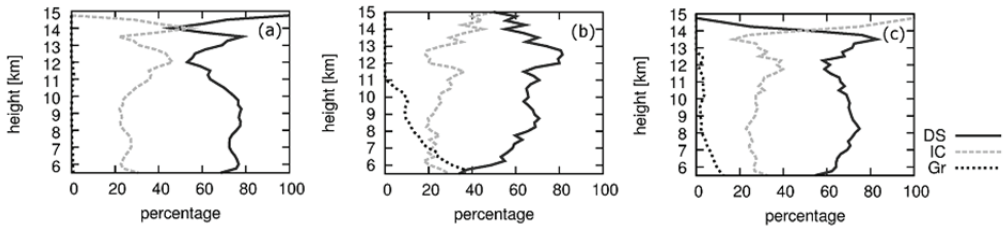

Fig. 4 : Vertical distributions of frequency of solid particles; ice crystal (gray broken line), dry snow (solid line), and dry graupel (dotted line) above a height of 5.5 km (around the melting level) for 3 types of the precipitation system: (a) a stratiform precipitation system, (b) an isolated convection, and (c) convective cells embedded in a stratiform precipitation system.

Structure of a mesoscale convective system observed in PALAU2013: A preliminary result

To clarify structure of mecoscale convective systems (MCSs) over the tropical ocean, we conducted an intensive field experiment in Republic of Palau in June 2013 (PALAU2013). Direct observations of ice particles using hydrometeor videosondes (HYVISs) were conducted within the observation ranges of a polarimetric radar and a Doppler radar. This study shows an overview of the field experiment and preliminary result in PALAU2013.

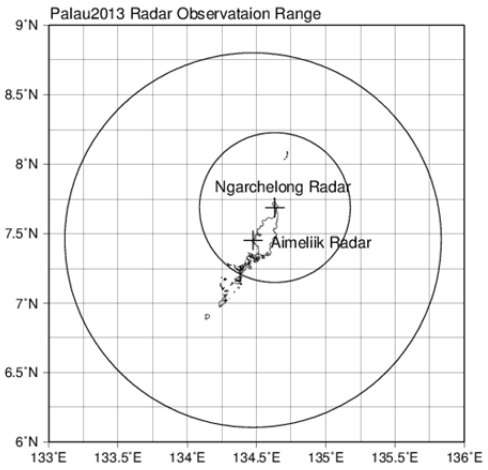

Fig. 5 : The location of radar sites and their observation ranges in Republic of Palau during PALAU2013.

An X-band polarimetric Doppler radar whose observation range is 60 km was installed at the northern tip of Palau, the Ngarchelong site (Fig. 5). Another X-band Doppler radar whose observation range is 150 km has already been installed at the Aimeliik site since 2004. Both radars made a continuous volume scanning observation at every 7.5 min. HYVIS observations were also conducted at the Aimeliik site. Totally 19 HYVISs were launched in PALAU2013.

HYVIS observations identify vertical profiles of ice particle's properties (type, size, and number concentration) as well as the height, air temperature, and humidity.

Passage of MCSs is detected by a large echo area (Fig. 6). Three MCSs that develop to typhoon T1303, T1304, and T1306 after the passage of the observation region are observed on June 06 (DOY=157), 15 (DOY=166), and 26 (DOY=177), respectively. A MCS accompanied leading convective and trailing stratiform regions with meridional length of 200 km and zonal width of 150 km propagated westward over the observation range of the radars on June 15. Four HYVISs were intermittently launched into the MCS. Figure 7 shows particle images at a height of 6.1 km of the first HYVIS launched just behind the convective region. Ice particles of column and plate types and a frozen drop as well as small particles of supercooled liquid water are found in this image.

We will make a dual-Doppler analysis to detect a vortex structure in a convection and a matching analysis on hydrometeor classification obtained by a polarimetric radar and HYVIS observations in near future.

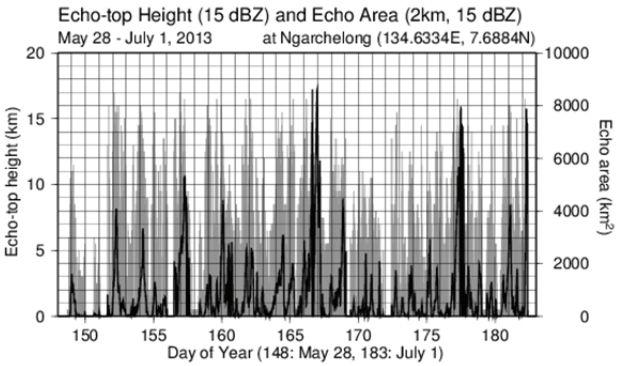

Fig. 6 : Time series of echo-top height (gray bar graph) and echo area at a height of 2 km (solid line) from May 28 (DOY = 148) to July 1 (DOY = 182), 2013. Both echo-top height and echo area are defined by 15 dBZ.

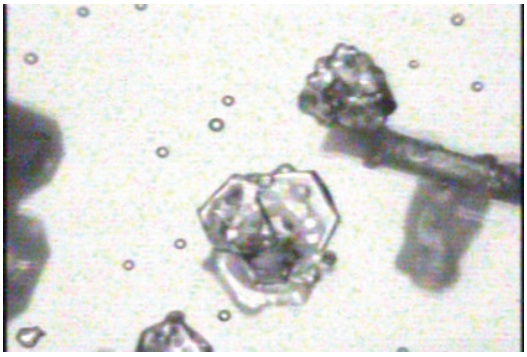

Fig. 7 : A particle image obtained by a HYVIS at a height of 6.1 km (temperature -5.2 Celsius degree) launched at 1445 LST from the Aimeliik Site, Republic of Palau. Horizontal and vertical scales of the image are 1.2 mm and 0.9 mm, respectively.

Evaluation of environmental modulators influencing the intensity change of a tropical cyclone using a coupled atmosphere-ocean non-hydrostatic model

Environmental modulators such as ocean heat content (OHC) and vertical wind shear (VWS) influence on the intensity change of tropical cyclones (TCs). Park et al. (2012; *Tropical Cyclone Research and Review*) showed that OHC and VWS influence the intensity change of TCs in terms of a two-dimensional phase diagram (hereafter PEH diagram) using reanalysis data of the atmosphere and ocean. However, they were not able to evaluate the relationship between them in comparison with many previous studies. In the present study, we try to evaluate the relationship between OHC and VWS for T1013 (Megi) using a coupled atmosphere-ocean non-hydrostatic model, Cloud Resolving Storm Simulator (CReSS) and Non-Hydrostatic Ocean model for Earth Simulator (NHOES), CReSS-NHOES with horizontal grid resolution of 0.02 degree both for latitude and longitude (approximately 2 km). The simulation is conducted for 7 days from 00 UTC on October 14, 2010, after one day of the formation of T1013.

The simulation well reproduces its track (not shown) and the tendency of central pressure (Fig. 8). The simulated minimum central pressure (889 hPa) corresponds to the observed one (885 hPa).

We define the inner core region of the TC as the maximum wind speed in the vertical column exceeds 25 m s^{-1}, thus the size of the inner core region is flexible. The atmospheric environment in which VWS between 850 and 200 hPa is estimated, is defined as the outer region in the range of 2 degrees of the inner core region. The oceanic environment in which OHC is calculated by heat content above the depth of 26 degree Celsius, is defined as the ocean below the inner core region. Figure 9 shows the PEH diagram obtained by the CReSS-NHOES simulation. In this diagram, the lower right (upper left) area shows high (low) OHC and low (high) VWS; that is favorite (not favorite) on the development of a TC. When T1013 intensifies (initial development period between Oct. 14 and 16, and rapid intensification period between 12 Z on Oct. 17 and 00 Z on Oct. 18), VWS is lesser than 6 m s^{-1} and OHC is larger than 90 kJ cm^{-2}. These environmental modulators are suitable for the intensification of TCs shown in previous studies. On the other hand, when T1013 maintains its intensity between 00 Z on Oct. 16 and 12 Z on Oct. 17, VWS increases above 7.5 m s^{-1} and OHC decreases below 90 kJ cm^{-2}. Using the PEH diagram, we reproduce well the relationship between these modulators and the intensification of T1013. In comparison with Park et al. (2012), the impact of the dynamical process around the center of TCs on the environment (VHS) should be needed to evaluate the intensity change of TCs. In addition, the interaction of TCs and ocean should be included to evaluate it.

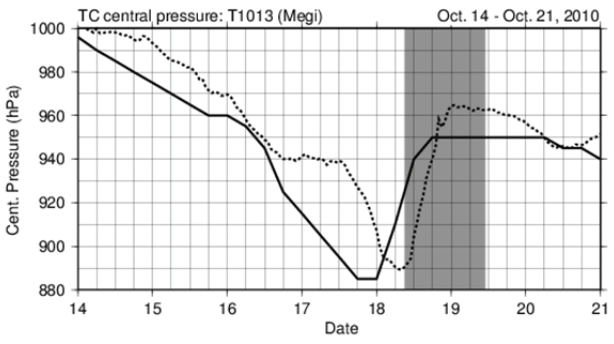

Fig. 8 : Time series of observed (solid line) and simulated central pressure of T1013. Gray shaded shows that T1013 landfall on Luzon Island, the Philippines.

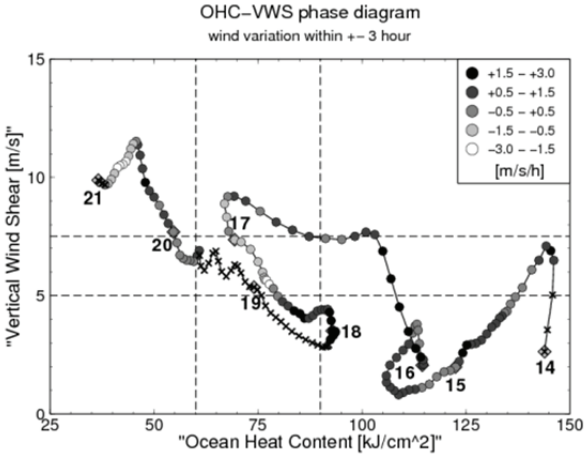

Fig. 9 : The PEH diagram using the CReSS-NHOES simulation on T1013. Horizontal and vertical axes show OHC and VWS, respectively. Intensification rate of the TC is calculated by 3 hours before and after the time. Dark and light gray marks show the intensification and decaying at the time, respectively. Crosses show the period when T1013 landfall on Luzon Island.

A formation mechanism of gust wind around a meso-β-scale vortex developed along the Japan-Sea Polar-airmass Convergence Zone during the cold-air outbreak

When cold-air outbreak occurs over the Sea of Japan during the winter season, meso-β-scale vortical disturbances (meso-β vortices), with horizontal scale of several tens km, are frequently observed along the Japan-Sea Polar-airmass Convergence Zone (JPCZ) by satellite images. The meso-β vortices are sometimes accompanied with the spiral and comma shaped radar echoes and bring about gust wind after their landing on the coastal region facing the Sea of Japan. However, a mechanism of its gust wind has been unclear, because it is difficult to observe the vortices over the sea; that is, their horizontal scale and lifetime are too small and short to observe. The purpose of the present study is to clarify the formation mechanism of gust wind related to the meso-β vortices using a cloud resolving model: Cloud Resolving Storm Simulator (CReSS). We performed a simulation with horizontal resolutions of 500 m on meso-β vortices observed on January 29, 2011.

Figure 10 shows simulated vertical integrated hydrometeor amount corresponding to cloud coverage of meso-β vortices over the Sea of Japan as well as the visible satellite image at 1430 JST on January 29, 2011. The model simulated well the cloud pattern over the Sea of Japan, and the position and scale of vortices along the JPCZ in comparison with the satellite image. The diameter and thickness of the meso-β vortices shown in "A" in Fig. 10 are approximately 100 km and 1.5 km, respectively. Time-height section of area averaged kinetic energy including the meso-β vortex "A" shows that the layer of maximum kinetic energy is found in the low-level and that of minimum appears around a height of 2 km above the top of the meso-β vortex (not shown). Another maximum layer is found above a height of 3.5 km, thus the low-level maxima of kinetic energy is clearly separated with the upper-level one. As a result, the origin of the gust wind around the surface in the meso-β vortex is not expected to be the advection of the high wind region from the upper-level.

A back trajectory analysis is examined to investigate the origin of the gust wind. Figure 11 shows time series of wind speed, kinetic energy, and pressure gradient force of air parcel intruding the gust wind region of the meso-β vortex along the back trajectory. The air parcel has its origin at a height of 1 km of the north and wind speed is small at that time. The wind speed accelerates as the air parcel approaches the meso-β vortex corresponding to the increase of pressure gradient force. Thus we concluded that the forming mechanism of gust wind around the meso-β vortex is the acceleration by pressure gradient force, not by the vertical advection of the high wind in the upper level.

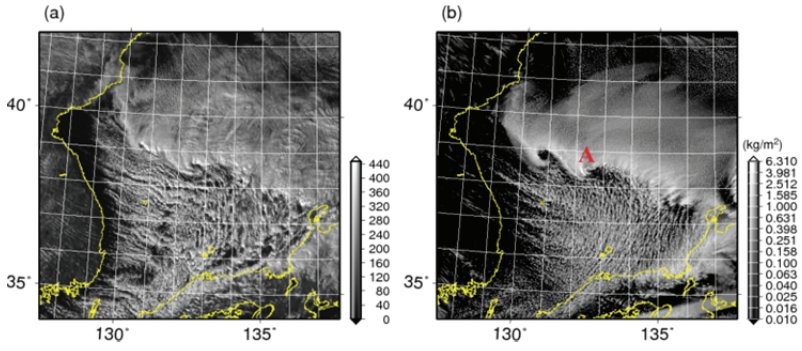

Fig. 10 : (a) Visible image over the Sea of Japan at 1430 JST on January 29, 2011. (b) Vertical integrated hydrometeor amount (kg m^{-2}) simulated by CReSS at the same time. White color shows the existence of high hydrometeor (dense cloud region).

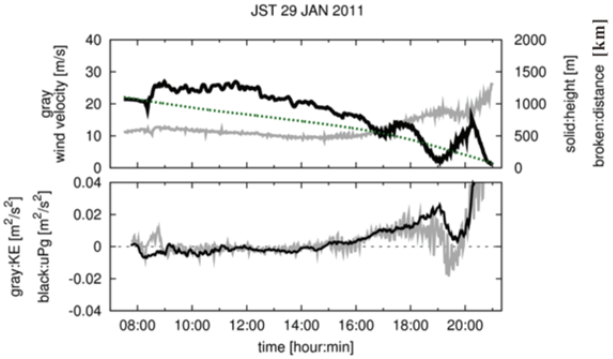

Fig. 11 : Time series of the back trajectory analysis starting at 2100 JST on January 29, 2011 calculated using the simulation result. The upper panel shows time series of wind speed (gray solid line), height (solid line), and distance from the starting position of the back trajectory (dotted line) of the air parcel. The lower panel shows time series of kinetic energy (gray solid line) and pressure gradient force (solid line) of the air parcel.

Impacts of GPS and Doppler radar data assimilation on precipitation prediction - A heavy rainfall event in the southern Gifu Prefecture on July 15, 2010 -

To Improve reproducibility of a numerical weather prediction on local heavy rainfall events, improving an initial condition should be needed. In particular, a moisture field is one of the less described variables in initial conditions because of its high spatial and temporal variability. The aim of the present study is to clarify the sensitivity of data assimilation of the moisture field on the location and amount of precipitation. We conduct a numerical simulation on a heavy rainfall event in the southern Gifu Prefecture on July 15, 2010 using Cloud Resolving Storm Simulator (CReSS) with horizontal grid resolution of 1 km. We cannot reproduce the rainfall distribution and maximum rainfall amount around the target region without assimilating Global Positioning System derived precipitable water vapor (GPS-PWV) and horizontal wind (HW) derived from Doppler radar. Three-dimensional variational data assimilation (3DVAR DA) system is used to investigate the impact of GPS-PWV. HW is also assimilated by nudging method. This study investigates the impact of three different GPS-PWV data such as "Near Real Time analysis (NRT)," "reanalysis," and "F3" data.

Figure 12 shows the impact of GPS-PWV and HW on the horizontal distribution of total precipitation amount for 9 hours starting from 18 JST on July 15, 2010. The location and amount of precipitation in the southern Gifu Prefecture is improved by assimilating both GPS-PWV and HW in comparison with no assimilation experiment (Fig. 12b). However, total precipitation amount is less than half of the observation. Application of sequential assimilation of GPS-PWV with nudging technique improve the reproducibility of total precipitation amount (Fig. 12c, 12d). It suggests that the sequential assimilation of GPS-PWV is quite useful to quantitative precipitation forecasting (QPF).

Figure 13 shows time series of hourly precipitation of each GPS-PWV assimilation as well as the observed one at Tajimi. Maximum precipitation and its peak time assimilating the "reanalysis" GPS data are reproduced better than those assimilating "NRT" and "F3" data. The "reanalysis" GPS data estimates more accurate PWV using a correct GPS satellite position relative to the Earth surface. However, it cannot release in real time since GPS orbit data before and after 30 days are needed to calculate. Thus the "reanalysis" GPS data cannot apply for the forecasting on heavy rainfall events. However, this result suggests that providing more accurate GPS-PWV data is expected to improve the forecasting on heavy rainfall events.

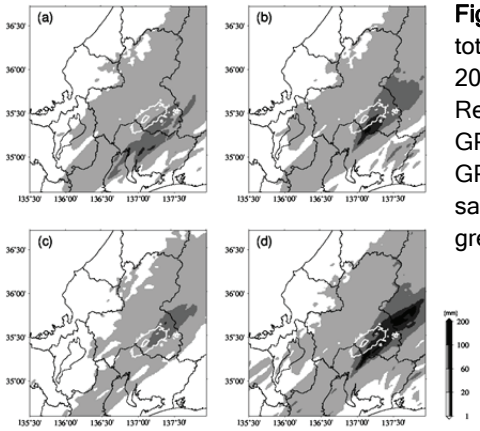

Fig. 12 : Sensitivity of GPS-PWV and HW on horizontal distributions of total precipitation amount for 9 hours starting from 18 JST on July 15, 2010. White contour shows that observed by JMA at every 100 mm. Result of (a) assimilating only GPS-PWV (NRT) data, (b) assimilating GPS-PWV (NRT) and HW data, (c) conducting sequential assimilation of GPS-PWV with nudging technique for all GPS observation points, and (d) same as (c) except for the GPS observation points that observed PWV is greater than the simulated one are drawn.

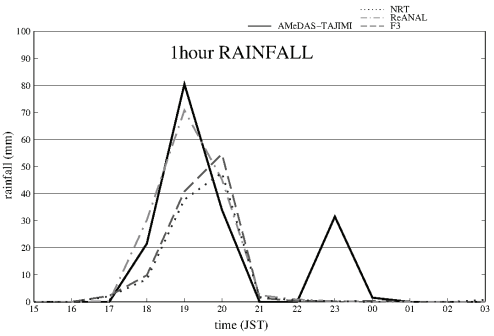

Fig. 13 : Time series of hourly precipitation of sequential assimilation of different method on GPS-PWV at a grid including Tajimi AMeDAS station. Observed series (solid line), assimilating "NRT" (dotted line), "reanalysis" (chain line), and "F3" (broken line) GPS data are drawn.

Laboratory for Cloud and Precipitation Climatology

A Mechanism of Tropical Convection Inferred from Observed Variability in the Moist Static Energy Budget

Temporal variability in the moist static energy (MSE) budget is studied with measurements from a coordination of different satellites including the Tropical Rainfall Measuring Mission (TRMM) and Afternoon Train (A-Train) platforms. A composite time series before and after the development of moist convection is obtained from the observations to delineate the evolution of MSE and moisture convergences and, in their combination, gross moist stability (GMS). A new algorithm is then applied to estimate large-scale vertical motion from energy budget constraints (Fig. 1) through a vertical mode decomposition into first and second baroclinic modes and a background-shallow mode.

The findings are indicative of a possible mechanism of tropical convection. A gradual destabilization is brought about by the MSE convergence intrinsic to the positive second baroclinic mode (congestus mode) that increasingly counteracts a weak MSE divergence in the background state (Fig. 2b). GMS is driven to nearly zero as the first baroclinic mode begins to intensify, accelerating the growth of vigorous large-scale updrafts and deep convection (Fig. 2c). As the convective burst peaks, the positive second mode switches to the negative mode (stratiform mode) and introduces an abrupt rise of MSE divergence that likely discourages further maintenance of deep convection. The first mode quickly dissipates and GMS increases away from zero, eventually returning to the background-shallow mode state. A notable caveat to this scenario is that GMS serves as a more reliable metric when defined with radiative heating rate included to offset MSE convergence.

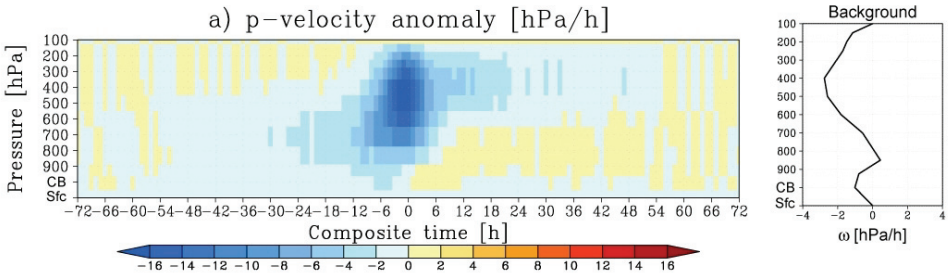

Fig. 1 : Composite time series of large-scale mean vertical velocity anomaly (hPa/h).

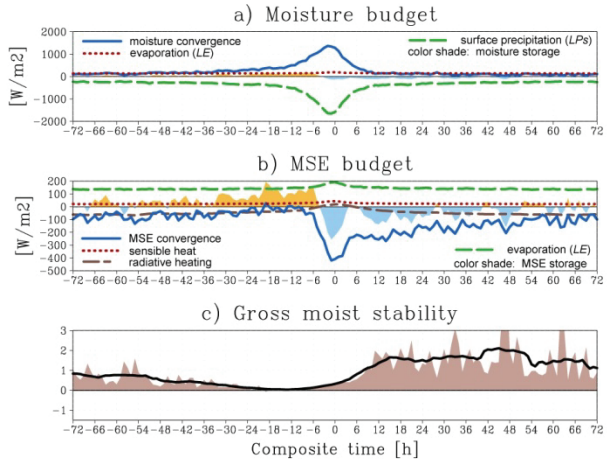

Fig. 2 : Composite time series of moisture and MSE budget parameters. (a) Moisture budget, (b) MSE budget, and (c) gross moist stability (GMS).

Reference: Masunaga, H., 2013: A Mechanism of Tropical Convection Inferred from Observed Variability in the Moist Static Energy Budget, *J. Atmos. Sci.*, in press.

A Satellite Study of Propagation Characteristics of Sea Surface Temperature associated with the Intraseasonal Oscillations

This study is aimed at understanding the potential roles of sea surface temperature (SST) variability associated with the Intraseasonal Oscillation (ISO) using various satellite data. A composite analysis of the ocean mixed-layer heat budget in term of ISO phases is performed for boreal winter and summer to examine the seasonal variation of ISO propagation. A warm SST anomaly preceding the propagation of an enhanced ISO convection from the Indian Ocean to the Maritime Continent (Fig. 3) mainly arises from the variability of shortwave and latent heat fluxes. An easterly anomaly to the east of convection diminishes scalar wind, and thus latent heat flux, when superposed onto a background westerly, implying that the presence of basic westerly wind is important for the development of a warm SST anomaly ahead of the ISO convection. The seasonal migration of background westerly, confined into a southern equatorial belt in boreal winter while spread across the north Indian Ocean in boreal summer (Fig. 4), may offer a mechanism that partly accounts for the seasonal characteristics of ISO propagation. The northward propagation of the SST variability associated with the boreal summer ISO is found to also involve a similar mechanism with the meridional wind modulation of scalar wind.

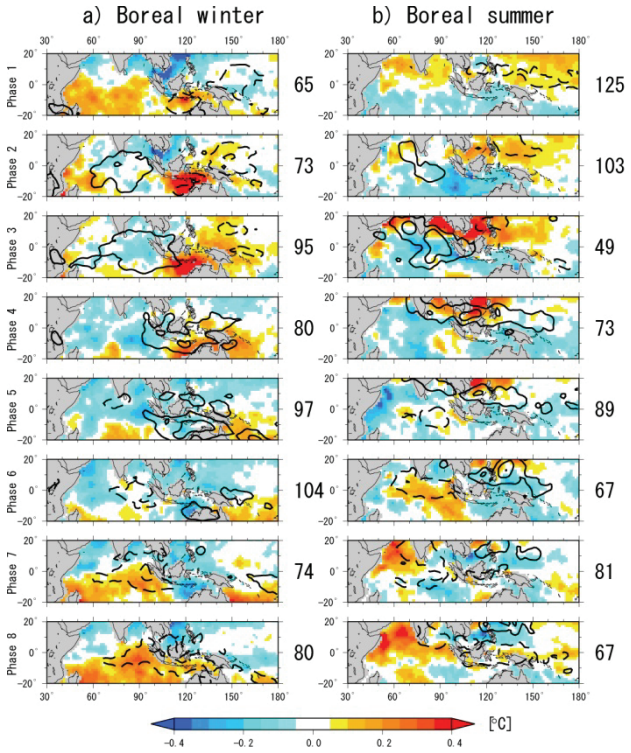

Fig. 3 : OLR (contour) and SST (shaded) anomalies for each MJO phase in (a) boreal winter and (b) boreal summer.

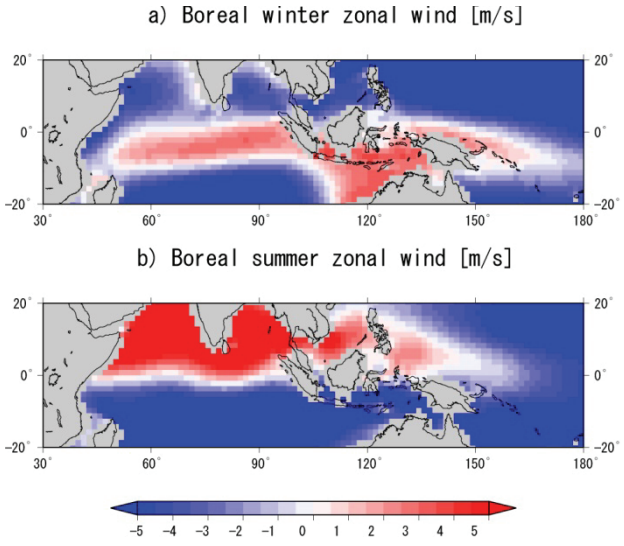

Fig. 4 : Climatology of surface zonal wind in (a) boreal winter and (b) boreal summer.

Reference: Kanemaru, K. and Masunaga, H., 2014: A Satellite Study of Propagation Characteristics of Sea Surface Temperature associated with the Intraseasonal Oscillations, *J. Climate*, in press.

Eco-Climate System Laboratory

Dynamics of distinct intraseasonal oscillation in summer monsoon rainfall over the Meghalaya–Bangladesh–western Myanmar region

This study investigated the detailed rainfall distribution related to the submonthly (7–25-day)-scale intraseasonal oscillation (ISO) around the Meghalaya–Bangladesh–western Myanmar (MBWM) region. The associated three-dimensional atmospheric circulation and time-evolution features were investigated for the whole Asian summer monsoon system from the tropics to the mid-latitudes using APHRODITE, TRMM-PR, and JRA25 reanalysis datasets.

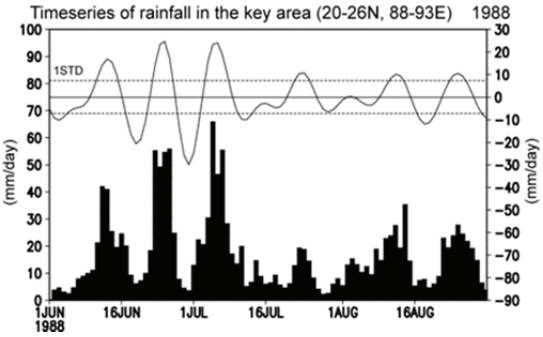

Fig1. Time series of rainfall averaged over the domain of 20°-26°N, 88°-93°E in 1988 (black bars; left axis) and 7-25-day filtered rainfall (solid line; right axis).

The MBWM region, where a tremendous amount of rainfall is observed in summer, is the most dominant area of submonthly-scale ISO among the Asian summer monsoon regions (Fig. 1). A distinct rainfall ISO is caused by the low level zonal wind fluctuations and its interaction with the regional-scale topographical features around the MBWM, with a remarkable alternation between westerly and easterly flow. In the active phase of the ISO over the MBWM, a low-level westerly/southwesterly prevails over the MBWM and a center of cyclonic vorticity appears over Bangladesh. Therefore, the wind components normal to the windward slopes of the Meghalaya Plateau, the Chittagong Hill Tracts, and the western coast of Myanmar are enhanced high rainfall is then observed over these regions due to the orographic lifting of moist air (Figs. 2a and 2c). Relatively high rainfall in the lowland area of the MBWM away from the regional-scale mountains is due to frictional convergence in the boundary layer under strong low-level cyclonic circulation. In contrast, the direction of moisture flow changes such that easterly/southeasterly flow prevails along the Gangetic Plain in the peak break phase (Figs. 2b and 2d). The easterly/southeasterly flow can travel along the Gangetic Plain

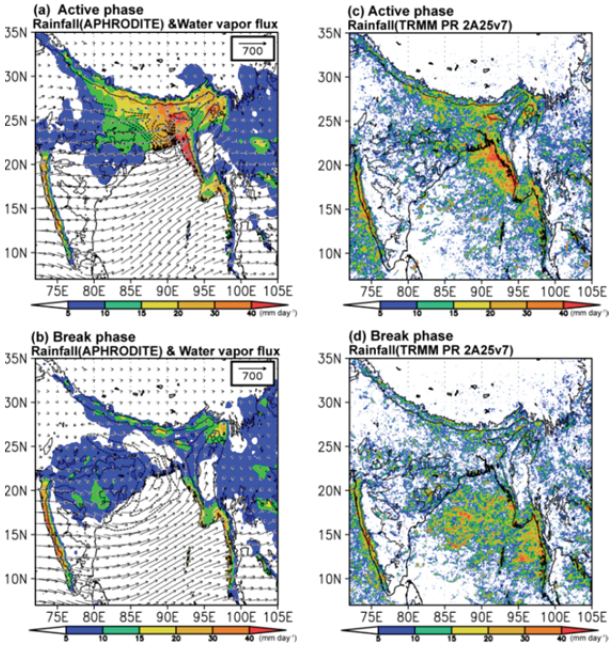

Fig 2. Composites of (a) rainfall (APHRODITE) and vertically integrated (from surface to 100 hPa) water vapor flux vectors in the peak active phase of the 7-25-day ISO over the MBWM. The contours of 925-hPa positive (i.e., cyclonic) vorticity more than 2.5 9 10-5 s-1 are shown by dotted lines. The topographic contours of 500 and 3,000 m are also shown as thin solid lines. (b) As in (a), but for peak break phase. (c) Composite of rainfall obtained from TRMM-PR in the active phase. (d) As in (c), but for the break phase.

from northwestern Bangladesh without orographic barriers. Thus, precipitation decreases significantly along the Gangetic Plain on peak break days.

The distinct alternation of the low-level zonal wind around the MBWM is caused by the westward propagating vortex pair with zonal wavenumber ~6 and westward phase speed of ~6.5 m s^{-1} in the tropics, which is consistent with the n = 1 equatorial Rossby (ER) wave. The centers of the vortices propagate westward along ~15°N and 5°S. Thus, the twin vortex structure of the ER wave shifts northward by 5°, likely due to the large north–south asymmetric nature of the ambient Asian summer monsoon circulation in the tropics (Fig. 3). The northern vortex can affect the MBWM region. As the anticyclonic vortex moves into the Bay of Bengal, the westerly/southwesterly becomes strengthened around the MBWM, which is covered by the northern fringe of the anticyclonic vortex. Additionally, the MBWM region is located in the easternmost part of the Gangetic Plain, an east–west flat lowland that is surrounded to the north and south by high-elevation areas (i.e., the Himalayas/TP and the Chota Nagpur Plateau). The topographic features of the Gangetic Plain enhance the zonal wind fluctuation, and westerly/southwesterly flow brings high rainfall on submonthly timescales around the MBWM.

Additionally, robust circulation signals relevant to the ISO appear over the mid-latitudes. In the upper troposphere, a wavetrain structure is evident along the Asian subtropical jet. The waves have a Rossby wavelike structure with a zonal wavenumber of ~4.5 and a westward phase speed relative to the ground of ~2.7 m s^{-1}, consistent with the theory of mid-latitude barotropic Rossby waves in terms of the zonal phase speed relative to the mean background wind. In addition to the slow westward propagation, the eastward development of the new center of action is observed along the Asian jet, indicative of Rossby wave energy dispersion along the waveguide of the Asian jet. The waves have barotropic vertical structure around the TP. In the active phase of the ISO over the MBWM, the cyclonic anomaly dominates throughout the troposphere around the TP (e.g. Fig. 3). This is associated with the deepening of the monsoon trough just to the south of the TP. Thus, the cyclonic anomaly to the south of the TP enhances the north–south pressure gradient and in turn enhances the westerly flow in conjunction with the anticyclonic anomaly over the Bay of Bengal. The robust circulation and convection signals relevant to the ISO extend across the whole Asian summer monsoon system from the tropics to the mid-latitudes over the MBWM region.

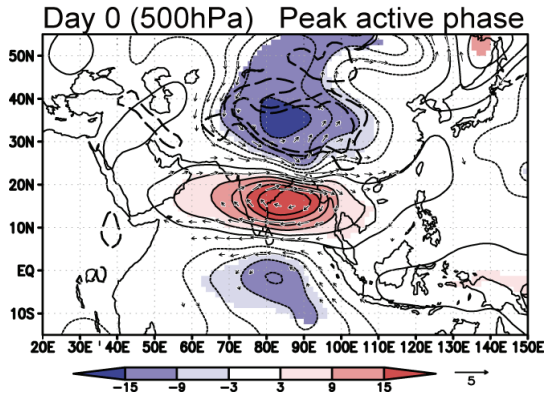

Fig. 3. Composite of the 500-hPa streamfunction (ψ) and wind vector anomalies at the peak active phase (day 0) with reference to the 7-25-day rainfall anomalies over the MBWM. Shaded areas correspond to areas of 99 % confidence in the ψ anomalies. Only wind vectors statistically significant at the 99 % level are plotted. The contours of topographic contours for 1,500 and 3,000 m are shown as dashed lines.

Reference : Fujinami, H., T. Yasunari and A. Morimoto, 2014: Dynamics of distinct intraseasonal oscillation in summer monsoon rainfall over the Meghalaya-Bangladesh-western Myanmar region : Covariability between the tropics and mid-latitudes, *Climate Dynamics*, in press.

Water and carbon cycling in Cambodian rubber plantations

Rubber (*Hevea brasiliensis* Müll. Arg.) plantations, which are rapidly expanding into both climatically optimal and sub-optimal environments throughout mainland Southeast Asia, potentially change the partitioning of water, energy, and carbon at multiple scales, compared with traditional land covers that are being replaced.

Eddy covariance towers were established within two rubber plantations, one each in Bueng Kan, northeastern Thailand, and Kampong Cham, central Cambodia, to measure ecosystem fluxes. The results show that evapotranspiration (ET) at both sites is strongly related to variations in available energy and leaf area, and moderately controlled by soil moisture. Measured mean annual ET was 1128 and 1272 mm yr^{-1} for the Thailand and Cambodia sites, respectively. After adjustment for energy closure, mean annual ET was estimated to be 1211 and 1459 mm yr^{-1} at the Thailand and Cambodia sites, respectively. Based on these estimates and that of another site in Xishuangbanna, southwestern China, it appears that ET of rubber is higher than that of other land covers in the region, including forest (Fig. 4).

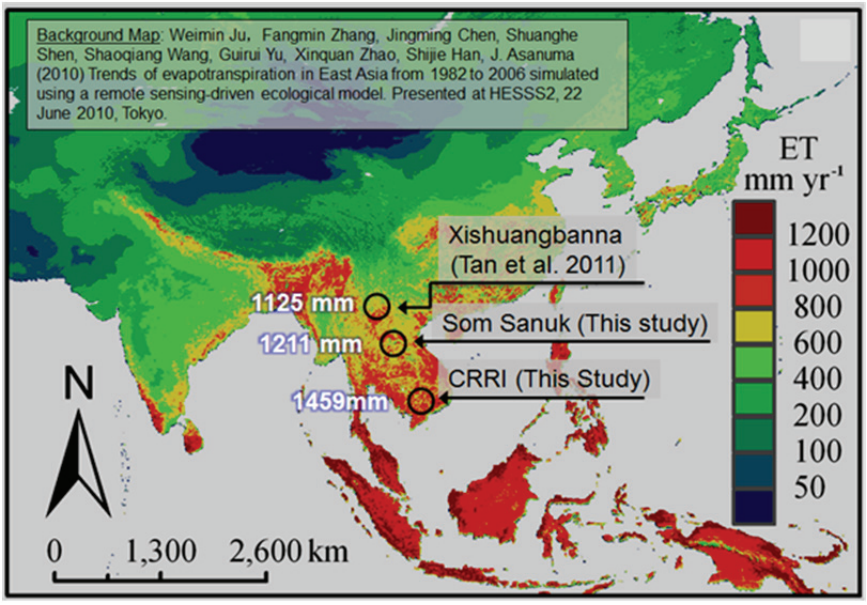

Fig4. Distribution of studied rubber plantation sites' annual evapotranspiration (ET) in the Southeast Asian tropics ET map. From Prof. Thomas W. Giambelluca at University of Hawaii at Manoa.

Sap flow measurements were used to study the intra- and inter-annual variations in transpiration rate (E_t) in a rubber stand in the lowlands of central Cambodia. Mean stand sap flux density (J_S) indicate rubber trees actively transpire in the rainy season, but become inactive in the dry season. A sharp, brief short-time drop in J_S synchronization occurred simultaneously with leaf shedding in the middle of the dry season in January. Although annual maxima of J_s were approximately the same in two experimental years, maximum daily stand E_t of ~ 2.0 mm day^{-1} in 2010 increased to ~ 2.4 mm day^{-1} in 2011. Stomatal response was well explained by changes in solar radiation, vapor pressure deficit, soil moisture availability, leaf area, and tree diameter. Rubber trees had a relatively small potential to transpire, compared with average diffuse-porous species in the beginning of study period. After two years of growth in tree diameter, transpiration potential was comparable to other species. Sensitivity of canopy conductance (g_c) to the atmospheric drought indicates isohydric behavior of rubber trees. Modeling also predicted relatively small sensitivity of g_c to the soil moisture deficit and rapid decrease in g_c under extreme drought conditions (Fig. 5). However, annual observations suggest the possibility of change in

leaf characteristics with tree maturity and/or initiation of latex tapping. Estimated annual stand E_t was 469 mm year^{-1} in 2010, increasing to 658 mm year^{-1} in 2011. Diagnostic experiments using the obtained g_c model showed that inter-annual change of stand E_t in the rapidly growing young rubber stand was determined mainly by the tree growth rate, not changes of air and soil variables in the surrounding environment. Future research should focus on the potentially broad applicability of the relationship between Et and tree size as well as environmental factors at stands different in terms of clonal type and age.

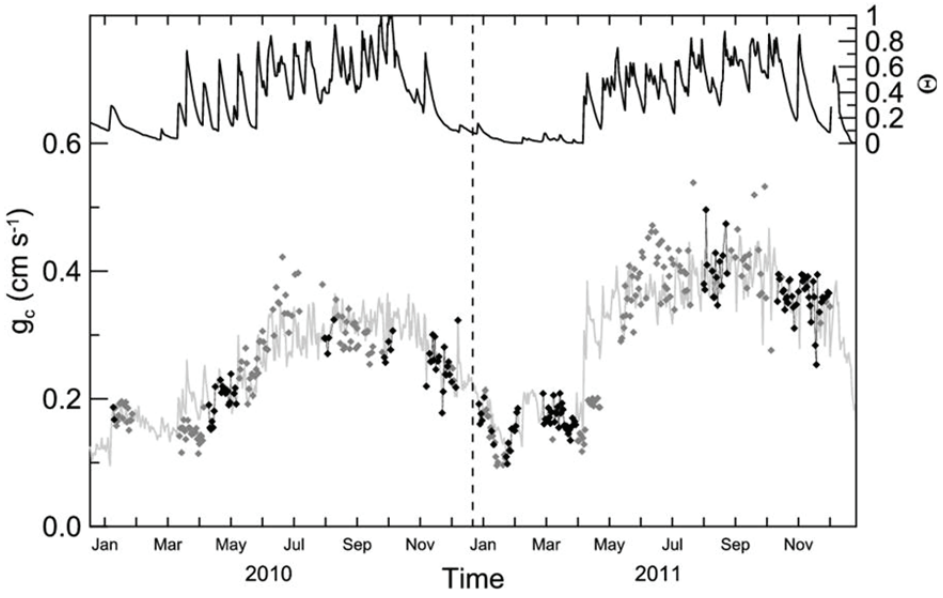

Fig5. Soil moisture (black solid line), canopy stomatal conductance estimated from sap flow measurements (closed circles) and their modeled values (gray line).

We developed a soil-vegetation-atmosphere transfer (SVAT) model applicable to simulating CO_2 and H_2O fluxes from the canopies of rubber plantations, which are characterized by distinct canopy clumping produced by regular spacing of plantation trees. Describing the biosphere-atmosphere exchange in rubber plantations via SVAT modeling is important to understanding the impacts on environmental processes. The regular spacing of plantation trees creates a peculiar canopy structure that is not well represented in most SVAT models, which generally assume a non-uniform spacing of vegetation. Herein we develop a SVAT model applicable to a rubber plantation and an evaluation method for its canopy structure, and examine how the peculiar canopy structure of rubber plantations affects canopy CO_2 and H_2O exchanges. Model results are compared with measurements collected at a field site in central Cambodia (Fig. 6). Our findings suggest that it is crucial to account for intensive canopy clumping in order to reproduce observed rubber plantation fluxes. These results suggest a potentially optimal spacing of rubber trees to produce high primary productivity and water use efficiency.

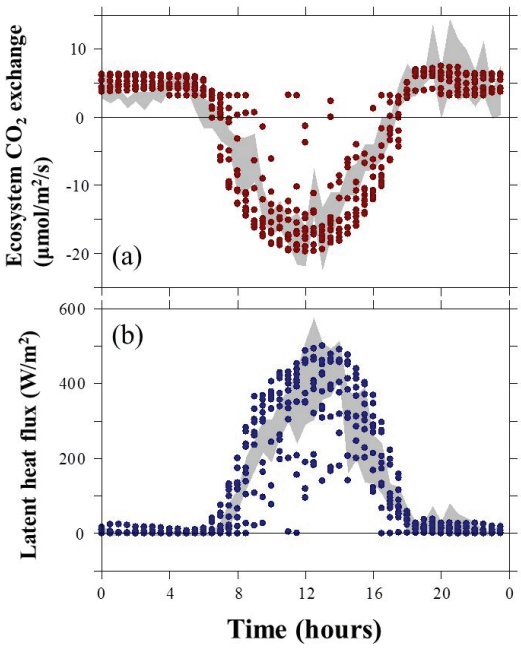

Fig6. Mean diurnal cycles of measured (gray zones) and modeled (solid circles) ecosystem CO_2 exchange (a) and latent heat flux (b) for 5-14 (10 days) August 2011. The gray zone denotes the range of the middle two quartiles of observations in the study period.

Deforestation-induced reduction in rainfall

A spatial distribution of atmospheric moisture convergence averaged over 1998-2010 in the eastern Pacific Ocean (built using a reanalyzed and gridded four-dimensional meteorology dataset, Japanese 25-year ReAnalysis (JRA-25) and the Japan Meteorological Agency (JMA) Climate Data Assimilation System (JCDAS) available via <http://jra.kishou.go.jp/JRA-25/index_en.html>) suggests less moisture convergence and divergence over Borneo compared with other regions (Fig. 7). On the other hand, the Tropical Rainfall Measuring Mission (TRMM) satellite measurements from 1998 to 2010 (NASA Goddard Earth Sciences (GES) Data and Information Services Center (DISC), available via <http://disc.sci.gsfc.nasa.gov/about-us>) showed a larger amount of precipitation above islands of the maritime continent in the western Pacific Ocean compared with sea areas, suggesting a notably large amount of precipitation over Borneo (Fig. 7). In short, while little atmospheric moisture horizontally moves into and out of the atmospheric space over Borneo, this area has plenty of precipitation.

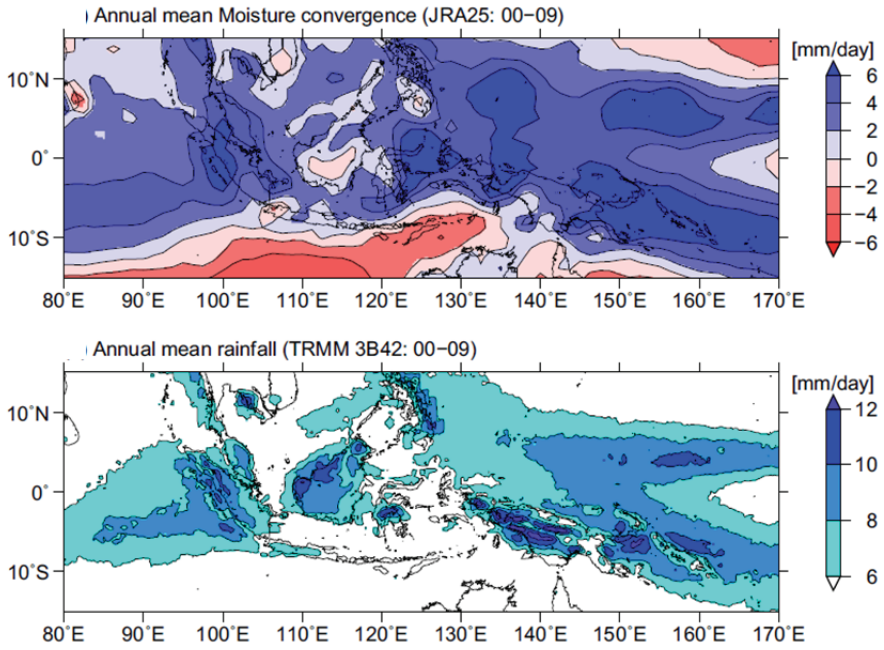

Fig7. Maps of (upper panel) annual mean moisture convergence and (bottom panel) annual mean precipitation in the western Pacific Ocean, (constructed using JRA-25 and Tropical Rainfall Measuring Mission (TRMM) satellite measurements 3B42 Ver.7 datasets, respectively with values averaged over the period 1998-2010).

Therefore, a question arises: where does water for precipitation come from? According to the atmospheric water budget equation, assuming that the time change of local available precipitable water content is negligible, annual evapotranspiration over Borneo was roughly estimated to be ~7 mm day^{-1} and balanced with the annual precipitation, implying that most of the precipitation was recycled from terrestrial evapotranspiration over Borneo. However, this evapotranspiration value surpassed the upper limit of the potential evaporation when taking into consideration basic meteorological variables in this region. The computation of the budget equation using the combination of the reanalysis and the satellite measurement data, which are different in their derivations, might cause such a discrepancy. Nevertheless, in light of comparisons with the other areas, it is certain that there are large amounts of precipitation, and little moisture advection into or out of, the Bornean region (Fig. 7). Also, a yearly eddy covariance

observation conducted at a Bornean tropical rainforest site indicated the high rate of pristine rainforest evapotranspiration, which can be approximated using the same mechanism as the evaporation from an extensive water surface, to be ~4 mm day^{-1} as an annual mean. Thus, we concluded that there is a higher ratio of recycling from terrestrial evapotranspiration into the precipitation over Borneo, and that deforestation and forest degradation could alter this eco-hydro-climatological cycling.

Therefore, it is plausible that the deforestation and forest degradation has led to a long-term decline in precipitation in Borneo, showed by the long-term daily grid precipitation datasets (APHRODITE's Water Resources, available via http://www.chikyu.ac.jp/precip/) over Borneo (Fig. 8). In addition, it was pointed out that a slowdown of the Walker circulation over the last 60 years suppressed moisture convergence over the maritime continent including Borneo, resulting in the historical decline in land precipitation. We argue that deforestation and forest degradation can be still a major factor inducing the decline in precipitation because such a weakening of moisture convergence would promote recycling of the terrestrial evapotranspiration into the precipitation.

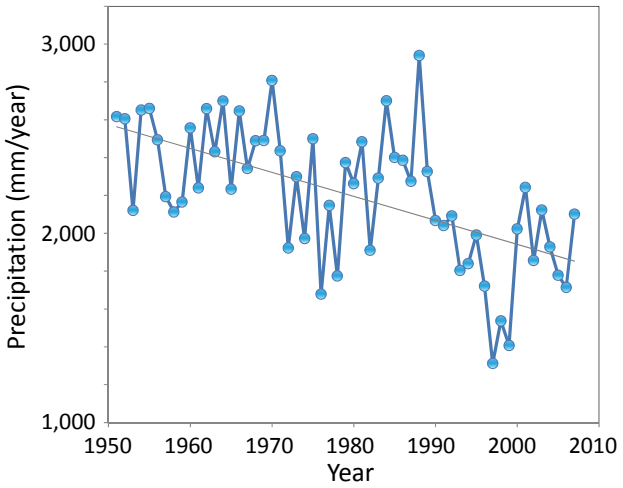

Fig8. The decreasing trend (-12.7 mm yr^{-1}) in annual precipitation integrated over Borneo, in the period 1951-2007. A significant regression line is also shown ($p < 0.0001$). Note that even though precipitation data in 1997 and 1998, when a strong El Niño event occurred and caused an extreme drought, were excluded, this decreasing trend was unchanged.

Laboratory of Satellite Biological Oceanography

Estimation of phytoplankton size fractions from light absorption spectra

Size structure of phytoplankton in aquatic environment is very important for biogeochemical processes such as food chain and material transport, and it is affected by environmental conditions such as river discharge. Here, we developed remote sensing algorithm to estimate phytoplankton size structure of marine environment. Most of the previously developed algorithms just focused on the open ocean, and rely on an assumption that small and large cells dominate in low and high chlorophyll *a* (Chl-*a*) waters, respectively (Brewin et al., 2010). However, this assumption is not always valid in river influenced coastal waters such as in the East China Sea (ECS) (Wang et al., 2014).

Light absorption spectra of phytoplankton should have great potential to retrieve the size structure because it is strongly depend on packaging effect caused by phytoplankton cell size and on different pigment composition related to phytoplankton taxonomy (Ciotti et al., 2002). In this study, we developed an estimation method of phytoplankton size-fractions which is applicable to coastal waters as well as open ocean using principal component analysis (PCA) of normalized light absorption spectra.

We measured phytoplankton absorption coefficient ($a_{ph}(\lambda)$) and High Performance Liquid Chromatograph (HPLC) pigment concentrations in the ECS, Tsushima Strait and Ise-Mikawa Bay. Remote sensing reflectance, $R_{rs}(\lambda)$, were also measured during some stations using an underwater spectral radiometer (PRR-800/810). Size-fractions of total phytoplankton Chl-*a* (Tchl-*a*) were derived from HPLC pigments by diagnostic pigment analysis (Hirata et al., 2008). $a_{ph}(\lambda)$ was normalized using four methods to remove total biomass influence; 1) divided by Tchl-*a* ($a_{ph}^{*}(\lambda)$), 2) divided by $a_{ph}(675)$ ($a_{ph}^{675}(\lambda)$), 3) divided by average of $a_{ph}(\lambda)$ ($a_{ph}^{ave}(\lambda)$), and 4) subtracted by the wavelength average and divided by the standard derivation of $a_{ph}(\lambda)$ ($a_{ph}^{std}(\lambda)$). PCA was used to capture spectral variations of the normalized $a_{ph}(\lambda)$ and separate the variance into uncorrelated principal component (PC). Then, empirical relationships between HPLC-derived size-fractions (f) and PC scores (S) were examined as following;

$$f = \frac{1}{1+\exp(\beta_0 + \sum_{i=1}^{n} \beta_i S_i)},$$

where f is the large (micro-) and small (pico-) phytoplankton fractions. S_i and n is the i th PC score and the number of PC which was four in this study, respectively. β_0 and β_i are the regression coefficients between f and S_i. For middle size (nano-) phytoplankton, the fraction (f_{nano}) was calculated as;

$$f_{nano} = 1 - f_{micro} - f_{pico}.$$

Applicability of the model satellite (MODIS) data was validated using $a_{ph}(\lambda)$ derived from *in situ* $R_{rs}(\lambda)$ by the version 5 of quasi-analytical algorithm (QAA).

$a_{ph}^{*}(\lambda)$ showed clear differences with changes of the phytoplankton size-fractions (Fig. 1). Samples with high fractions of micro-phytoplankton displayed low $a_{ph}^{*}(\lambda)$ because of the high packaging effect, whereas $a_{ph}^{*}(\lambda)$ of samples with high pico-phytoplankton fractions were high due to the low packaging effect. The packaging effect of nano-phytoplankton dominated samples were medium, and moderate $a_{ph}^{*}(\lambda)$ were seen for these samples. The micro-phytoplankton dominated samples showed flat spectra and a shoulder around 450–470 nm. On the contrary, the spectra of samples dominated by pico-phytoplankton were sharp and showed a lifting at about 490 nm.

The PCA clearly separated the variations of $a_{ph}^{*}(\lambda)$ into different PC modes, and the first four modes contained 94.1%, 3.1%, 1.1% and 0.6% of the variance. Phytoplankton size-fractions estimated from the first four PC scores agreed well with those derived from HPLC pigments (Fig. 2). Comparisons of the

PCA model performance between the four normalized $a_{ph}(\lambda)$ revealed that the PCA model was robust for the normalization method and that $a_{ph}^{std}(\lambda)$ was slightly better than other three normalized $a_{ph}(\lambda)$. Therefore, $a_{ph}^{std}(\lambda)$ derived from *in situ* $R_{rs}(\lambda)$ at only MODIS bands was used to validate the model performance, and the results showed that the PCA model could derive an acceptable accuracy with R^2 of 0.85, 0.61 and 0.76 and RMSE of 0.130, 0.126 and 0.112 for micro-, nano- and pico-phytoplankton fractions, respectively. This indicates that if the adequate atmospheric correction can be achieved, the PCA approach can map phytoplankton size-fractions from satellite observations. Furthermore, we applied the PCA approach to the NASA bio-Optical Marine Algorithm Dataset (NOMAD) which were collected from the global ocean. The results showed that the PCA approach was also applicable to the global ocean.

In conclusion, the PCA approach proposed in this study could derive an acceptable estimation of phytoplankton size-fractions from absorption spectra both in coastal waters and global ocean. Next step of the study should focus on the practicability of the PCA approach for real satellite observations.

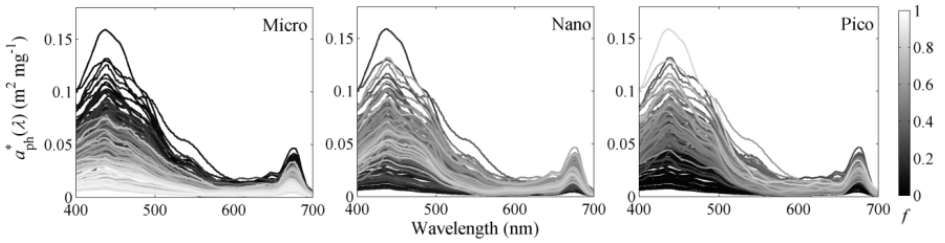

Fig. 1 : Spectra of $a_{ph}^*(\lambda)$ for all samples. Gray levels indicate size fractions (f) of micro-, nano- and pico-phytoplankton.

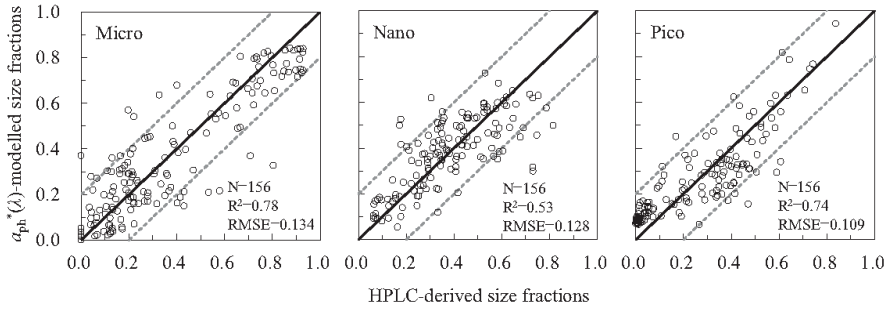

Fig. 2 : $a_{ph}^*(\lambda)$-modelled versus HPLC-derived size fractions. Black lines indicate the 1:1 line, and grey dashes indicate the ± 0.2 fraction ranges relative to the 1:1 line.

Transport of giant jellyfish, *Nemopilema nomurai*, in Yellow Sea and East China Sea

Outbreaks of giant jellyfish, *Nemomilema nomurai,* have been a serious problem for the fisheries of northeast Asian countries, especially Japan, China, and Korea, in 2000s. Abundance of the giant jellyfish in the Yellow Sea (YS), East China Sea (ECS), and the Sea of Japan was high during the summer. However, the benthic stage, polyp, of the giant jellyfish was not found in the field. The initial floating stage separated from the polype, ephyrae, were found only one time offshore of Jiangsu coast in May. The young jellyfish was found in the ECS and Tsushima Strait in June (Kawahara et al., 2006; Yoon et al., 2008), and relatively large adults (diameter >30 cm) was captured in the Sea of Japan in August. It is expected that the benthic stage is in the coast of the YS and ECS and that the floating stage is transported to offshore by current. However, it remains unclear how the ephyrae and young medusae is transported and distributed in the different water masses. The main objectives of this study were to investigate the distribution of young medusae with the relationship to water mass expressed as seawater temperature and salinity, to understand the transport of the jellyfish by current, and furthermore to identify the possible source area using ship observations, satellite data, and a particle-tracking experiment with model flow fields.

Based on the temperature and salinity properties in the surface during the cruises in July 2013, eight main water masses were identified by the cluster analysis; Changjiang Diluted Water (CDW), South Yellow Sea Water Mass (SYSW), North Yellow Sea Water Mass (NYSW), Taiwan Warm Current water mass (TWC), Kuroshio Warm Current water mass (KWC), Changjiang mouth Upwelling Water mass (CUW), mixed water of CDW-TWC, and mixed water of CDW-KWC. The jellyfish were mostly concentrated in YS and northern ECS water, and hardly observed in the south ECS water.

Results of the backward trajectories of water masses by flow field of JCOPE2 in YS, which reflected the modeled flow pattern, indicated that the coastal current flow northward, northward or northeastward, and eastward in May, June and July, respectively (Fig. 3 b, d and f). The this modeled flow pattern was consistent with wind-driven current. Satellite SST data also indicated that the warm water (>15 ^{o}C) intruded north or northeastward to the offshore of YS from May to July (Fig. 3 a, c and e). Majority of water masses (particle No. 2, 3, 4 and 7) in the southern YS with high abundance of jellyfish were back traced to Jiangsu coast in early May (Fig. 3 b, d and f), when the 15^{o}C isotherm was formed near the traced position (Fig. 3 a, c and e). While, water masses without jellyfish were staying in the offshore of the YS, or traced back Changjiang mouth inlet and Taiwan Strait. The inconsistency of model salinity to the field data indicates that the backward trajectories of CDW were questionable. However, transport of jellyfish from the Jiangsu coast in early May was verified by the forward tracking experiments and an independent ferry boat observation data.

The study based on the young medusa available to visual observation in July with coupling of satellite data and particle tracking experiment provided a possible source area of the medusa. The high abundance of giant jellyfish observed in YS in July probably transported by wind-driven currentfrom the north of the Changjiang mouth to northern Jiangsu coast in May when ephyrae were liberated from polyps after SST became higher than 15^{o}C.

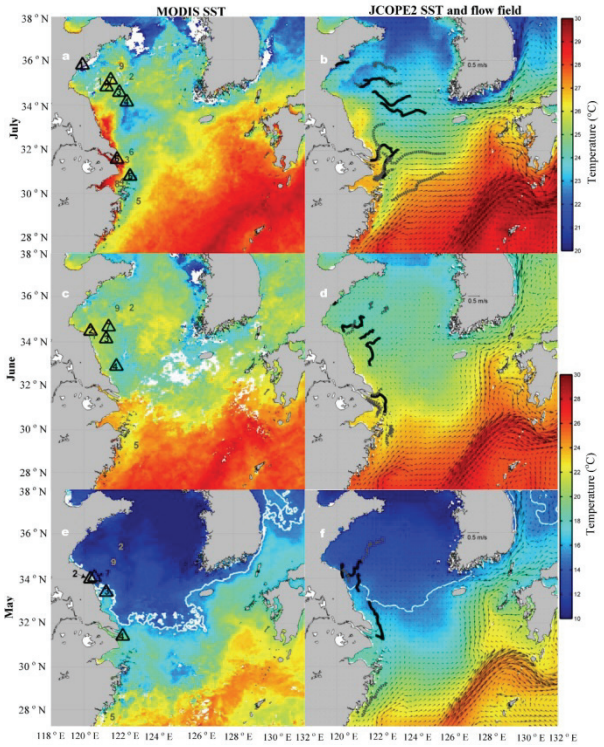

Fig. 3 : MODIS monthly mean SST (a, c, e) and monthly mean SST/flow fields of JCOPE2 model (b, d, f) from July to May 2013. Numbers in a, c, and e were the final positions of the particle-tracking experiments of water masses in each month with (△) and without (no mark) jellyfish. Black and grey lines in b, d, and f indicate backward trajectories of water masses during the month with and without jellyfish, respectively. White line indicates the 15℃ isotherm.

Biogeochemical responses associated with the passage of a cyclonic eddy in the western North Pacific

The primary productivity in the subtropical region was considered to be low due to the low concentration of nutrients in the surface layer. However, the possibility of nutrient supply into the surface layer associated with mesoscale perturbations such as eddies are pointed out recently. We conducted a shipboard high-resolution hydrographic survey in the subtropical region of the western North Pacific from October to November 2008 and found part of a cyclonic eddy around 30oN, 145oE (Figure 4). This eddy had propagated westward with an average transit speed of 7 cm s-1 in the region south of the Kuroshio Extension for at least 6 months as a wavelike disturbance (Figure 5). Within this eddy, isopycnals shallowed between a depth of 600 m and just below the surface mixed layer. In addition, maximal dissolved oxygen concentrations were observed in the subsurface layer between depths of 50 and 100 m (Figure 6). Nitrate was depleted within this subsurface maximal oxygen layer.

These results suggest that nutrients in the deeper layers were supplied into the euphotic layer as a result of the uplift of isopycnals in the eddy, fueling the photosynthesis of phytoplankton in the subsurface and emitting an excess of oxygen due to new production. Compared with the outside of the eddy, the enhancement of oxygen and the decrease of nitrate in the center of the eddy were estimated to be 2.7 mol O2 m–2 and 0.22 mol N m–2, respectively. The primary productivity calculated using the eddy speed was 650 mg C m–2 d–1 at the center of the eddy. The enhanced primary productivity due to the passage of the eddy is likely to have an important role in the ecosystem and on material cycling in the subtropical region.

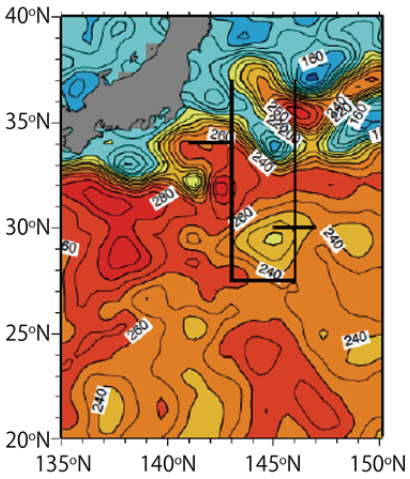

Fig.4 : The altimetric sea surface height map southeast of Japan on 22 October 2008. Thick black lines indicate the hydrographic sections of the KH-08-3 cruise leg 2.

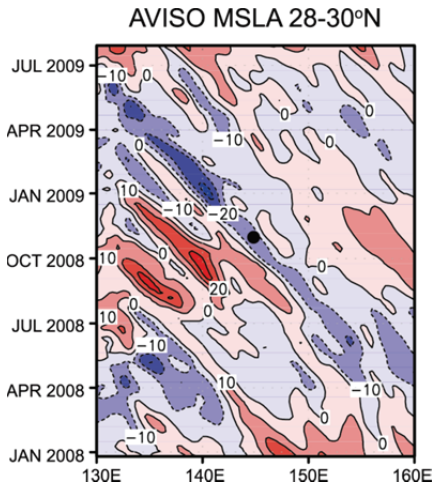

Fig.5 : Time series of sea surface height anomalies along the zonal band of 28-30oN. A black dot indicates the position and time of the shipboard observation.

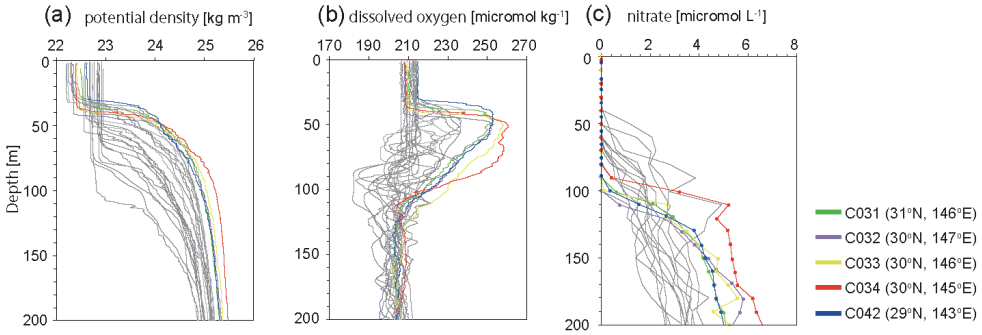

Fig.6 : Vertical profiles of (a) potential density, (b) dissolved oxygen concentration, (c) nitrate concentration. Colored and gray lines are the profiles for stations inside and outside the eddy, respectively.

Loboratory of Bio-Physical Oceanography

Interannual variation in the third branch of the Tsushima Warm Current path controlled by winter surface cooling in the Japan Sea

In order to investigate interannual variation in the third branch of the Tsushima Warm Current (TBTWC) path in the Japan Sea, EOF, correlation, and lag correlation analysis are applied to a monthly mean absolute sea surface dynamic heights (ASSDH) data with high spatial-temporal resolution. These analyses suggest as follows. A subarctic circulation is intensified by stronger winter cooling compared to normal year, and then more amount of cold water mass is transported to off Korean coast by the current. As a result, the cold water mass off Korean coast expand in wider area. The TBTWC adjusts the density distribution off Korean coast and separates from the coast at lower latitude. There might be time lag between intensification of the subarctic circulation current and transport of cold water mass to off Korean coast.

The relationship between change of separation position of the TBTWC in summer and that of surface cooling in winter is explained as follows by a reduced gravity model. Stronger surface cooling in winter makes increase of upper layer thickness along north coast. Hence subarctic circulation in spring is intensified. Intensified subarctic circulation transports cold water mass to the south along west coast. Since southward flow along west coast in strong surface cooling year in winter is faster than that in normal sea surface cooling year in winter, deeper upper layer thickness expand to more south in summer with cold water mass (Fig. 1). Consequently, the northward current (TBTWC) along west coast in strong sea surface cooling year separates at lower latitude than that in normal sea surface cooling year in summer time.

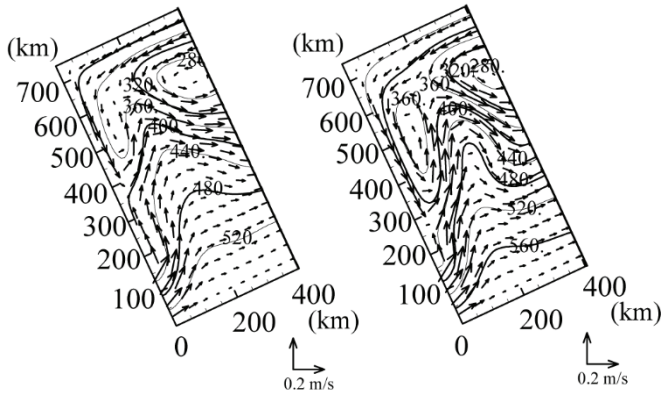

Fig. 1 : Sea surface current and pressure distribution of model result in summer. Vectors show current and contour lines show pressure. Dashed line allows indicate the third branch of the Tsushima Warm Current path.

Development of tidal assimilation model for altimetry data

Satellite altimetries have been observed sea surface height continuously since 1992. Assuming geostrophic balance, sea surface currents are calculated and temporal and spatial variation of the sea surface currents are revealed from altimetry data. However, accuracy of the altimetry data are not sufficient in the marginal seas where tidal amplitude is large and tidal phenomena is complicated because of inaccurate tidal model. It is well-known that altimetry data in the Yellow and East China Seas include large error related with tidal model error. In the present study, we developed tidal assimilation model for accuracy improvement of altimetry data in the Yellow and East China Seas. We used the Princeton Ocean

Model. The model is 2 dimensional and grid size of the model is 1/36 degree. We calculated tidal amplitude and phase lag of 8 principal tidal constituents by the model. The model is constrained by tidal variation at open boundaries which is calculated NAO99Jb model, and sea level variation derived from altimetry data and tide gauge data in Japan, Korea, and China are assimilated into the model. Table 1 shows errors of the present model and NAO99Jb for each tidal constituent.

Error of the present model for each tidal constituent was less than 2 cm and total error of 8 principal constituents were 8.7 cm which was fewer than half of the number of NAO99Jb. Total error of the present model was approximately 5 cm in the area where water depth is more than 10 m. The error of 5 cm allows us to calculate sea surface current from altimetry data.

Table 1. Errors of the present model and NAO99Jb for 8 principal tidal constituents. Unit in cm.

Tidal constituents	M_2	S_2	O_1	K_1	Q_1	P_1	K_2	N_2	Total
Present model	1.6	0.8	1.5	1.6	0.8	1.2	0.6	0.7	8.7
NAO99Jb	3.8	2.1	2.9	3.4	0.9	1.1	2.3	1.2	17.7

Investigation of air-sea flux and its variation over the Kuroshio Extension region

Advanced Microwave Scanning Radiometer 2/Global Change Observation Mission 1st for Water: AMSR2/GCOM-W1 developed by JAXA was launched successfully in May 2012 and its observations were started from July 2012. Validation of AMSR2 is one of significant missions because the satellite sensor remotely observes ocean surface and its accuracy is unknown. The first time validation of AMSR2 standard products with in-situ observations was conducted over the ocean, particularly in the Kuroshio Extension region as a collaborative study with JAXA. Comparison with in-situ observations for a year, we could confirm that AMSR2 observation is fine and accuracy meets a criteria for standard data release: SST: 0.8℃, SSW: 1.5m/s (see Figure). AMSR2 ocean standard products promise to provide us good information for air-sea interaction, climate, and water cycle studies.

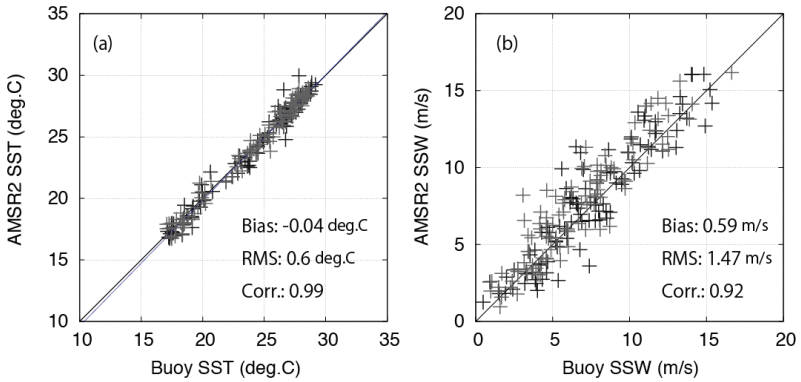

Fig. 2 : Scatter-diagrams between KEO buoy (x-axis) and AMSR2 (y-axis) for (a) sea surface temperature (SST, deg.C) and (b) sea surface wind speed (SSW, m/s).

Endowed Research Division

Stakeholder Management Research Laboratory

Since the Great East Japan Earthquake of 2011, there has been great concern on expanding the use of renewable energy. However, in order for the actual construction of offshore wind farms to be executed, the nation-level macro perspective of moving away from dependence on fossil fuels and nuclear power generation is not sufficient and the micro perspective of building consensus among local stakeholders is necessary. In addition, looking to the coastal areas closely involved with offshore wind farms, additional problems have become apparent including population decline and the aging of local fishermen, and the revitalization of fishing communities has emerged as an important challenge. If the introduction of offshore wind farms can be used not only for the purposes of supplying power but also as a mean of revitalizing local communities, we believe this will contribute not only to the spread and expansion of offshore wind power generation itself, but also to the restoration of regional vitality. This study suggests methods for achieving mutually beneficial relationships between local communities and offshore wind power.

While some demonstration offshore wind projects have taken place in Japan, no large-scale facilities have yet been built by the private sector. For this reason, there remains insufficient basic research for building the consensus necessary for moving forward with offshore wind projects. For example, there is little knowledge of the positive and negative impacts of the wind farm on the fishing industry. It is also not clear that which stakeholders need to be involved. We are conducting fieldwork in association with projects in four Japanese communities planning offshore wind power generation projects. In 2013, we carried out primarily interview-based investigation of local issues through discussions with coastal fishermen. We found that a resource-management fishery based in part on the use of offshore wind turbines constituted one method that might resolve local challenges. However, due to the possibility of interference with particular fishing methods (e.g., trawlnets), as well as that the sites of offshore wind farms might serve as shelter areas for ships, we came to the new realization of a future need to coordinate views with differently positioned stakeholders such as offshore fishermen. In addition, as we have built a collaborative relationship with Statoil ASA, who have developed large-scale offshore wind power generation projects in Europe, and with DNV GL, a firm that provides risk management services, we are collecting information on European methods for generating consensus and investigating the possibility of adapting these to Japan. Furthermore, we have been selected for the project by NEDO in “Research and Development of Wind and Renewable Energy Technology - Research and Development of Offshore Wind Power Technology - Basic Research For Local Co-Existence with Offshore Wind Farms (FY2013-2014)”, with future plans to conduct research on coexistence and harmony with coastal communities on top of local fishing industries.

Our outreach activities have included hosting seminars and symposiums on offshore wind power generation and participating in workshops held by the Royal Norwegian Embassy in Tokyo in order to introduce the stakeholder management research and share the knowledge of rules for marine utilization (e.g. fishing rights). In addition, in terms of university educational initiatives, we have been running “Environmental Innovation” as part of the Education for Sustainable Development (ESD) Program managed by the five graduate schools of environmental studies, and visiting researchers and others in our endowed research division have been offering lectures on energy-centered initiatives in the private sector. We also invited Statoil ASA, who is our research collaborator, to take part in our HyARC Seminar, which

focused on the themes of environmental impact assessment and floating offshore wind turbine development.

Fig. 1 : First symposium “Offshore wind projects and stakeholder management”

Fig. 2 : The floating offshore wind project of Statoil “Hywind”

Fig. 3 : Sheringham Shoal offshore wind farm

List of Publications

*:Staffs, students and research fellows in the HyARC.

January, 2013～March, 2014

№	Author	Title	Journal	Volume	Page doi	Date
1	Ferraro, R., C. Peters-Lidard , C. Hernandez, F. J. Turk, F. Aires, C. Prigent, X. Lin, S.-A. Boukabara, F.A. Furuzawa, K. Gopalan, K. Harrison, F. Karbou, L. Li, C. Li, H. Masunaga, L. Moy, S. Ringerud, G. Skofronik-Jackson, Y. Tian, and N.-Y. Wang	An evaluation of microwave land surface emissivities over the continental United States to benefit GPM-era precipitation algorithms.	IEEE Transactions on Geoscience and Remote Sensing	51	378 - 398 doi:10.1109/TGRS.2012.2199121	2013/1/1
2	Ueyama, M., K. Ichii, H. Iwata, E.S. Euskirchen, D. Zona, A.V. Rocha, Y. Harazono, C. Iwama, T. Nakai, W.C. Oechel	Upscaling terrestrial carbon dioxide fluxes in Alaska with satellite remote sensing and support vector regression.	Journal of Geophysical Research: Biogeosciences	108	1266-1281 doi: 10.1002/jgrg.20095	2013/1/1
3	Li, W., T. Hiyama, N. Kobayashi	Seasonal Variations of the Surface Fluxes and Surface Parameters over the Loess Plateau in China.	Atmospheric and Climate Sciences	3	111-120	2013/1/30
4	Igarashi,Y., N. Tanaka, T. Yoshifuji, C. Sato, C. Tantasirin and M. Suzuki	Seasonality of water and carbon dioxide exchanges at a teak plantation in northern Thailand.	Ecohydrology	6(1)	125-133	2013/2/1
5	Siswanto, E., J. Ishizaka, S.C. Tripathy, K. Miyamura	Detection of harmful algal blooms of *Karenia mikimotoi* using MODIS measurements: A case study of Seto-Inland Sea, Japan.	Remote Sensing of Environment	129(15)	185-196	2013/2/15

April, 2014～March, 2015

№	Author	Title	Journal	Volume	Page doi	Date
1	Ichikawa, K., W.C. Yang, A. Morimoto, Y. Yoshikawa, S. Sugitani, W.S. Chiang, J.W. Lai, E.Y. Liang, C.T. Liu, C.W. Lee, K. Yufu, M. Kyushima, S. Fujii, T. Senju, Y. Ide	Preliminary results of the Japan-Taiwan joint survey on combining ocean radar data in the Kuroshio upstream region.	Ocean Science Journal	48(1)	141-148	2013/4/1
2	Takahashi, D., A. Morimoto	Mean field and annual variation of surface flow in the East China Sea as revealed by combining satellite altimeter and drifter data.	Progress in Oceanography	111	125-139	2013/4/1
3	Imaoka, K. and K. Nakamura	Statstical Analysis of Temporal Variation of Heating Profiles Associated with Isolated Tropical Cold Cloud Systems by Using Satellite Observations.	Scientific Online Letters on the Atmosphere (SOLA)	9	51-55 doi:10.2151/sola.2913-012	2013/4/19

№	Author	Title	Journal	Volume	Page doi	Date
4	M. Rafiuddin, H. Uyeda, M. Kato	Development of an arc-shaped precipitation system during the pre-monsoon period in Bangladesh.	Meteorology and Atmospheric Physics	120,3-4	165-176 doi: 10.1007/s00703-013-0244-x	2013/5/1
5	Yamaguchi, H., J. Ishizaka, E. Siswanto, Y.B. Son, S. Yoo, Y. Kiyomoto	Seasonal and spring interannual variations in satellite-observed chlorophyll-a in the Yellow and East China Seas: New datasets with reduced interference from high concentration of resuspended sediment.	Continental Shelf Research	59	1-9	2013/5/15
6	Nakai, T., Y. Kim, R.C. Busey, R. Suzuki, S. Nagai, H. Kobayashi, H. Park, K. Sugiura, A. Ito	Characteristics of evapotranspiration from a permafrost black spruce forest in interior Alaska.	Polar Science	7	136–148	2013/6/1
7	Park, H., J.E. Walsh, Y. Kim, T. Nakai, T. Ohata	The role of declining Arctic sea ice in recent decreasing terrestrial Arctic snow depths.	Polar Science	7	174-187	2013/6/1
8	Sugiura, K., S. Nagai, T. Nakai, R. Suzuki	Application of time-lapse digital imagery for ground-truth verification of satellite indices in the boreal forests of Alaska.	Polar Science	7	149-161	2013/6/1
9	Nagai, S., T. Nakai, T.M. Saitoh, R.C. Busey, H. Kobayashi, R. Suzuki, H. Muraoka, Y. Kim	Seasonal changes in camera-based indices from an open canopy black spruce forest in Alaska, and comparison with indices from a closed canopy evergreen coniferous forest in Japan.	Polar Science	7	125-135	2013/6/1
10	Kanemaru, K. and H. Masunaga	A satellite study of the relationship between sea surface temperature and column water vapor over tropical and subtropical oceans.	Journal of Climate	26	4204-4218	2013/6/1
11	Maeshiro, R., B. Kusumoto , S. Fujii, T. Shiono and Y. Kubota	Using tree functional diversity to evaluate management impacts in a subtropical forest.	Ecosphere	4(6)	1-17 doi:org/10.1890/ES13-00125.1	2013/6/1
12	Sun, W.-Y., O. M. Sun and K. Tsuboki	A modified atmospheric non-hydrostatic model on low aspect ratio grids: part II.	Tellus Tellus Series A-Dynamic Meteorology and Oceanography	65A	19681	2013/6/28
13	Panicker, A. S., D. I. Lee, Y. V. Kumkar, D. Kim, M. Maki and H. Uyeda	Decadal climatological trends of aerosol optical parameters over three different environments in South Korea.	International Journal of Climatology	33(8)	1909-1916	2013/6/30
14	Kanamori, H., T. Yasunari, and K. Kuraji	Modulation of the Diurnal Cycle of Rainfall Associated with the MJO Observed by a Dense Hourly Rain Gauge Network at Sarawak, Borneo.	Journal of Climate	26	4858-4875	2013/7/1

№	Author	Title	Journal	Volume	Page doi	Date
15	Yamazaki, T., K. Kato, T. Ito, T. Nakai, K. Matsumoto, N. Miki, H. Park, T. Ohta	A common stomatal parameter set used to simulate the energy and water balance over boreal and temperate forests.	Journal of Meteorological Society of Japan	91	273-285	2013/7/1
16	Tomita, H., S-P. Xie, H. Tokinaga, and Y. Kawai	Cloud response to the meandering Kuroshio Extension front.	Journal of Climate	26(23)	9393-9398 doi:org/10.1175/JCLI-	2013/7/19
17	Wang, S., J. Ishizaka, H. Yamaguchi, S.C. Tripathy, M. Hayashi, Y. Xu, Y. Mino, T. Matsuno, Y. Watanabe and S. Yoo	Influence of river discharge on phytoplankton absorption properties: a case study in the East China Sea and Tsushima Strait.	Biogeosciences Discuss	10	14475-14514 doi:10.5194/bgd-10-14475-2013	2013/8/1
18	Masunaga, H.	A satellite study of tropical moist convection and environmental variability: A moisture and thermal budget analysis.	Journal of the Atmospheric Sciences	70	2443-2466 http://dx.doi.org/10.1175/JAS-D-12-0273.1	2013/8/1
19	Kumagai, T., R.G. Mudd, Y. Miyazawa, W. Liu, T.W. Giambelluca, N. Kobayashi, T.K. Lim, M. Jomura, K. Matsumoto, M. Huang, Q. Chen, A. Ziegler and S. Yin	Simulation of canopy CO2/H2O fluxes for a rubber (Hevea brasiliensis) plantation in central Cambodia: the effect of the regular spacing of planted trees.	Ecological Modelling	265	P124-135	2013/9/1
20	Kataoka, R., Y. Miyoshi, K. Shigematsu, D. Hampton,Y. Mori, T. Kubo, A. Yamashita, M. Tanaka, T. Takahei, T. Nakai, H. Miyahara, K. Shiokawa	Stereoscopic determination of all-sky altitude map of aurora using two ground-based Nikon DSLR cameras.	Annals of Geophysics	31	1543-1548	2013/9/1
21	Chiwa, M., T. Enoki, N. Higashi, T. Kumagai and K. Otsuki	The increased contribution of atmospheric nitrogen deposition to nitrogen cycling in a rural forested area of Kyushu, Japan.	Water, Air, & Soil Pollution		224:1763	2013/10/1
22	Xu, Y., J. Ishizaka, H. Yamaguchi, E. Siswanto and S. Wang	Relationships of interannual variability in SST and phytoplankton blooms with giantjellyfish (*Nemopilema nomurai*) outbreaks in the Yellow Sea and East China Sea.	Journal of Oceanography	69(5)	511-526 doi: 10.1007/s10872-013-0189-1	2013/10/1
23	Hamada, S., T. Tanaka, T. Ohta	Impacts of land use and topography on the cooling effect of green areas on surroundig urban areas.	Urban Forestry & Urban Greening	12(4)	426-434	2013/11/1
24	Saito, T., H. Matsuda, M. Komatsu, Y. Xianga, A. Takahashic, Y. Shinohara, K. Otsuki	Forest canopy interception loss exceeds wet canopy evaporation in Japanese cypress (Hinoki) and Japanese cedar (Sugi) plantations.	Journal of Hydrology	507	287-299	2013/12/1

№	Author	Title	Journal	Volume	Page doi	Date
25	Li, X., W.-K. Tao, H. Masunaga, G. Gu, and X. Zeng	Aerosol effects on cumulus congestus population over the tropical Pacific: A cloud-resolving modeling study.	Journal of the Meteorological Society of Japan	91	817-833	2013/12/1
26	Kumagai, T., H. Kanamori and T. Yasunari	Deforestation-induced reduction in rainfall.	Hydrological Processes	27(25)	3811-3814	2013/12/15
27	Kumagai, T., M. Tateishi, Y. Miyazawa, M. Kobayashi, N. Yoshifuji, H. Komatsu and T. Shimizu	Estimation of annual forest evapotranspiration from a coniferous plantation watershed in Japan (1): Water use components in Japanese cedar stands.	Journal of Hydrology	508	66-76	2014/1/1
28	Yoshifuji, N., Y. Igarashi, N. Tanaka, K. Tanaka, T. Sato, C. Tantasirin, M. Suzuki	Inter-annual variation in the response of leaf-out onset to soil moisture increase in a teak plantation in northern Thailand.	International Journal of Biometeorology	online first		2014/1/1
29	Lee, K.-O., H. Uyeda, Dong-In Lee	Microphysical structures associated with enhancement of convective cells over Mt. Halla, Jeju Island, Korea on 6 July.	Atmospheric Research	135-136	76-90	2014/1/1
30	Fujinami, H., T. Yasunari and A. Morimoto	Dynamics of distinct intraseasonal oscillation in summer monsoon rainfall over the Meghalaya-Bangladesh-western Myanmar region : Covariability between the tropics and mid-latitudes.	Climate Dynamics		doi: 10.1007/s00382-013-2040-1	2014/1/25
31	Umezawa, Y., A. Yamaguchi, J. Ishizaka, T. Hasegawa, C. Yoshimizu, I. Tayasu, H. Yoshimura, Y. Morii, T. Aoshima, and N. Yamawaki	Seasonal shifts in the contributions of the Changjiang River and the Kuroshio Current to nitrate dynamics in the continental shelf of the northern East China Sea based on a nitrate dual isotopic composition approach.	Biogeosciences	11(4)	1297-1317 doi:10.5194/bg-11-1297-2014	2014/2/1
32	Ito, M., A. Morimoto, T. Watanabe, O. Katoh, T. Takikawa	Tsushima Warm Current paths in the southwestern part of the Japan Sea.	Progress in Oceanography	121	83-93	2014/2/1
33	Tian, Y., C. Peters-Lidard , K. W. Harrison, C. Prigent, H. Norouzi, F. Aires, S.-A. Boukabara, F. A. Furuzawa and H. Masunaga	Quantifying uncertainties in land surface microwave emissivity retrievals.	IEEE Transactions on Geoscience and Remote Sensing	52	829-840	2014/2/1
34	Kobayashi, H., R. Suzuki, S. Nagai, T. Nakai, Y. Kim	Spatial scale and landscape heterogeneity effects on FAPAR in an open canopy black spruce forest in interior Alaska. IEEE Trans.	Geoscience and Remote Sensing Letters, IEEE	11	564-568	2014/2/1
35	Terauchi, G., R. Tsujimoto, J. Ishizaka, H. Nakata	Preliminary assessment of eutrophication by remotely sensed chlorophyll-a in Toyama Bay, the Sea of Japan.	Journal of Oceanography		doi:10.1007/s10872-014-0222-z	2014/2/18

№	Author	Title	Journal	Volume	Page doi	Date
36	Mino, Y., S. Matsumura, T. Lirdwitayaprasit, T. Fujiki, T. Yanagi, T. Saino	Variations in phytoplankton photo-physiology and productivity in a dynamic eutrophic ecosystem: a fast repetition rate fluorometer-based study.	Journal of Plankton Research	36 (2)	398-411	2014/3/7
37	Ohigashi, T., K. Tsuboki, Y. Shusse, H. Uyeda	An Intensification Process of a Winter Broad Cloud Band on a Flank of the Mountain Region along the Japan-Sea Coast.	Journal of the Meteorological Society of Japan	92	71-93 doi:10.2151/jmsj.2014-105	2014/3/14
38	Kobayashi, N., Kumagai, T., Miyazawa, Y., Matsumoto, K., Tateishi, M., Lim, T. K., Mudd, R. G., Ziegler, A., Giambelluca, T. W. and Yin, S.	Transpiration characteristics of a rubber plantation in central Cambodia.	Tree Physiology	34(3)	285-301	2014/3/18
39	Lee, K.-O., H. Uyeda and D.-I. Lee	Effect of an isolated elliptical terrain (Jeju Island) on rainfall enhancement in a moist environment.	Tellus TELLUS SERIES A-DYNAMIC METEOROLOGY AND OCEANOGRAPHY	66	doi:http://dx.doi.org/10.3402/tellusa.v66.20484	2014/3/19

Hydrospheric Atmospheric Research Center (HyARC)
Nagoya University

Furo-cho, Chikusa-ku, Nagoya 464-8601, Japan

Office:

Telephone: +81-52-789-3466

Facsimile: +81-52-788-6206

Home Page: http://www.hyarc.nagoya-u.ac.jp

The 2013 Annual Report was published October 2014 by the Hydrospheric Atmospheric Research Center (HyARC) Nagoya University.


HyARC
Hydrospheric Atmospheric Research Center, Nagoya University